



**HAL**  
open science

# Heavy halogen impact on Raman water bands at high pressure: Implications for salinity estimations in fluid inclusions

Tobias Grützner, Hélène Bureau

► **To cite this version:**

Tobias Grützner, Hélène Bureau. Heavy halogen impact on Raman water bands at high pressure: Implications for salinity estimations in fluid inclusions. *Chemical Geology*, 2024, 654, pp.122065. 10.1016/j.chemgeo.2024.122065 . hal-04560527

**HAL Id: hal-04560527**

**<https://hal.science/hal-04560527>**

Submitted on 26 Apr 2024

**HAL** is a multi-disciplinary open access archive for the deposit and dissemination of scientific research documents, whether they are published or not. The documents may come from teaching and research institutions in France or abroad, or from public or private research centers.

L'archive ouverte pluridisciplinaire **HAL**, est destinée au dépôt et à la diffusion de documents scientifiques de niveau recherche, publiés ou non, émanant des établissements d'enseignement et de recherche français ou étrangers, des laboratoires publics ou privés.

1            Heavy halogen impact on Raman water bands at high pressure:  
2                            implications for salinity estimations in fluid inclusions

3 Tobias Grützner<sup>1,2,3\*</sup>, Hélène Bureau<sup>1</sup>

4

5 <sup>1</sup> Institut de Minéralogie, de Physique des Matériaux et de Cosmochimie (IMPMC), Sorbonne  
6 Université Paris, France.

7 <sup>2</sup> Research School of Earth Sciences, Australian National University, Canberra, Australia.

8 <sup>3</sup> Institut für Geowissenschaften, Goethe-Universität Frankfurt, Germany.

9

10 \*Corresponding author

11

12 Email addresses: tobias.gruetzner@outlook.com (T. Grützner), helene.bureau@sorbonne-  
13 universite.fr (H. Bureau).

14

15

16 Abstract

17 We present a new experimental dataset on the impact of the heavy halogens chlorine, bromine  
18 and iodine on the Raman water bands concerning pressure and their concentration at room  
19 temperature. These experiments were conducted at ambient temperature, with variations in  
20 halogen concentration and pressure ranging from 0 to 1.4 GPa.

21 The strength of the Raman water band shift change increases with the ionic size from chlorine,  
22 over bromine, to iodine. Our experiments further demonstrate that increased pressure  
23 diminishes the impact of the halogen shift change to a varying extent for each of the three  
24 halogens. This finding can have significant implications for the salinity calculation of fluid  
25 inclusions in minerals such as quartz or olivine. Particularly in the low salinity range, the  
26 concentration can be markedly underestimated if the pressure effect is neglected. For  
27 experiments in diamond anvil cells involving halogens dissolved in water, the change in Raman  
28 water band shifts can serve either as a new tool to monitor pressure, or to monitor the salinity.

29

30

31 Keywords

32 Raman, water bands, Fluid inclusion, halogens, salinity, high pressure

33

## 34 1. Introduction

35 Halogens play a pivotal role as volatile elements, significantly impacting geodynamic  
36 processes. They constitute essential components of volcanic fumaroles and volcanic ejecta.  
37 Upon release into the atmosphere, halogens contribute to ozone destruction. In crustal  
38 hydrothermal fluids, halogen complexes (e.g., in saline fluids, brines, or molten salts) serve as  
39 major agents for metal transport in ore-forming processes related to hydrothermal systems  
40 (e.g., Aiuppa et al., 2009). Samples of such fluids can be found entrapped as inclusions in  
41 minerals like quartz (e.g., Brooks et al., 2019; Pankrushina et al., 2020) or olivine (e.g.,  
42 Kawamoto et al., 2013) in magmatic and metamorphic rocks. Raman spectroscopy has been  
43 employed for decades to determine the salinity of fluid inclusions, especially those too small  
44 for other common techniques like microthermometry – a method that determines salinity by  
45 observing and measuring the freezing temperature of the fluid (cf. e.g., Kawamoto et al., 2013;  
46 Moncada and Bodnar, 2012; Brooks et al., 2019).

47 The Raman spectra of water and aqueous fluids exhibit several peaks closely grouped at 2800-  
48 3800  $\text{cm}^{-1}$ , resulting in water stretching bands (e.g., Ratcliffe and Irish, 1982; Sun, 2009;  
49 Walrafen et al., 1986). In salty solutions or brines, halogen ions interact with the bonds of water  
50 molecules. Although ions and ionic bonding cannot be directly detected with Raman  
51 spectroscopy, their impact on the network of covalent water bonding is detectable. This effect  
52 has been the subject of numerous studies, with a substantial focus on chlorine (e.g., Dubessy  
53 et al., 2002; Durickovic et al., 2010; Georgiev et al., 1984; Mernagh and Wilde, 1989;  
54 Pankrushina et al., 2020; Sun, 2012; Sun et al., 2010; Tepstra et al., 1990) and, to a lesser  
55 extent, on the heavy halogen bromine (e.g., Tepstra et al., 1990). Halogen anions widen the  
56 water bonding network, forcing the network to change its bonding structure by favoring a  
57 certain type of bonding over others. A shift in water bands can be observed, correlating with  
58 the number of dissolved halogens and facilitating the determination of salt concentration in the  
59 solution or in mineral fluid inclusions (e.g., Dubessy et al., 2002; Durickovic et al., 2010;  
60 Georgiev et al., 1984; Mernagh and Wilde, 1989; Pankrushina et al., 2020; Sun, 2012; Sun et  
61 al., 2010; Tepstra et al., 1990).

62 The heavy halogens bromine and iodine possess a larger ionic size than chlorine. Their anions  
63 stretch the water network as much or even more than chlorine, causing a more pronounced  
64 alteration of the Raman shift (Tepstra et al., 1990). The impact of the cations (e.g., calcium,  
65 magnesium, sodium, potassium) in a salty solution seem to be negligible (Sun et al., 2010).

66 Two other factors can alter the shape of Raman water bands: (1) temperature (e.g.,  
67 Krishnamurthy et al., 1983; Ratcliffe and Irish, 1982) and (2) pressure (Romanenko et al.,  
68 2018). Increasing temperature has a similar effect to increasing halogen concentrations,  
69 enhancing the resulting peak at around  $3430\text{ cm}^{-1}$ . Pressure shifts the bands in the opposing  
70 direction: It decreases the peak at  $3430\text{ cm}^{-1}$  and increases the peak at  $3240\text{ cm}^{-1}$ .

71 While fluid inclusions in minerals are typically studied at ambient temperature and its effect  
72 can be ignored, the pressure in mineral fluid inclusions, such as those in quartz, is likely to be  
73 elevated, potentially impacting the Raman spectrum. In this study, we present a novel  
74 experimental dataset examining the impact of all three heavy halogens — chlorine, bromine,  
75 and iodine — on Raman water bands concerning pressure and halogen concentration at room  
76 temperature. We further compare our results to some natural fluid inclusion samples from other  
77 studies to demonstrate and constrain the impact of our dataset on natural fluid inclusions.

78

## 79 2. Experimental setup and methods

80 Various concentrations of NaCl, NaBr, or NaI salts were dissolved in water to synthesize salty  
81 solutions as starting materials (Table 1). Sodium-halogen salts exhibit excellent solubility in  
82 water, and sodium serves as the dominant cation in seawater-related fluids. Despite the  
83 seemingly negligible impact of cations (Sun et al., 2010), sodium was selected as the cation  
84 for all three halogens to mitigate cation effects and focus on the influence of the three halogen  
85 anions.

86 The experiments were conducted using a Chervin-type hydrothermal diamond anvil cell  
87 (HDAC) with a pressure-driving membrane (Chervin et al., 1995). The HDAC was equipped

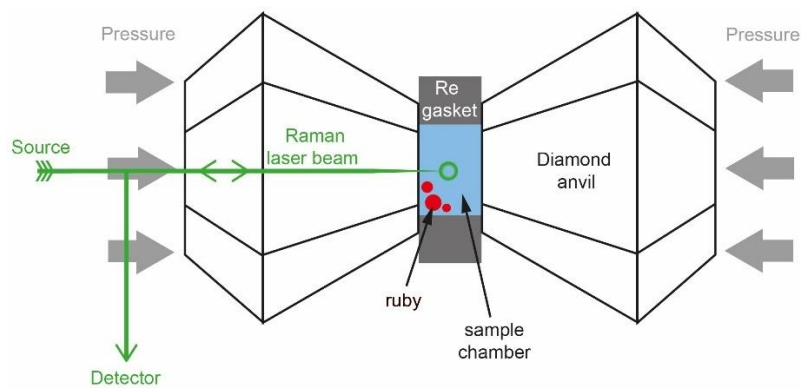
88 with 2 mm thick diamonds and culets of 1 mm diameter. The sample chamber, compressed  
89 between two diamonds, had a diameter of 500  $\mu\text{m}$ , drilled as a hole into a Re gasket with an  
90 initial thickness of 200  $\mu\text{m}$ . Before each experiment, the sample chamber was cleaned with  
91 ethanol, dried, and loaded with a salty solution along with a small number of ruby spheres for  
92 pressure calibration. Following HDAC closure, the membrane was connected to an inflator with  
93 a  $\text{N}_2$  gas bottle. The membrane was initially loaded with approximately 10 to 15 bar of gas  
94 pressure, sufficient to seal the HDAC but insufficient to observe a fluorescence shift with the  
95 ruby spheres.

96 Ruby fluorescence serves as a widely used pressure monitor for various DAC experiments  
97 (e.g., Chervin et al., 2001; Shen et al., 2020). The ruby shift was calibrated with the Raman to  
98 ambient pressure and had to be recalibrated for each new sample. After the ruby calibration,  
99 the water bands were measured with the Raman at ambient pressure. The pressure was then  
100 increased stepwise with an inflator, and pressure increases were monitored on the ruby  
101 fluorescence. Pressure steps were approximately 0.2 to 0.3 GPa. Depending on the salt  
102 concentration, the solution transforms into ice IV between 1.1 and 1.4 GPa (see below). After  
103 each pressure increase, the cell equilibrated the pressure for about 10 minutes before Raman  
104 analysis.

105 Raman measurements were performed with a 514.5 nm Argon laser and a Jobin-Yvon Horiba  
106 HR460 spectrometer. A constant grating of 1500 lines/mm, a slit size of 50  $\mu\text{m}$ , and a 50x  
107 objective placed in front of the diamond anvil cell were used. The setup was calibrated with a  
108  $521\text{ cm}^{-1}$  silicon wafer, and the laser energy was controlled to remain constant at 10 mW  
109 between each measurement during the pressure equilibration period. Diamond has no effect  
110 on the Raman water bands and is widely used for these types of studies. Test runs for pure  
111 water in the DAC and in a glass cylinder showed no difference in the spectra. Measurements  
112 in the solution were conducted in the center of the sample chamber by defocusing the laser  
113 spot between both surfaces of the two diamonds. Measurements in the solution were set for  
114 10 to 30 seconds with 3 to 5 iterations. Measurements on the ruby spheres were conducted  
115 "live" with a repetition rate of 1s.

116 It is important to note that halogens like iodine can also induce a Raman peak at around 1650  
117  $\text{cm}^{-1}$  (Besemer et al., 2016). However, this peak overlaps with the (extremely large) carbon  
118 peak from the diamond anvils and cannot be used for hydrothermal DAC experiments or for  
119 pressure calibration with HDAC.

120 The acquisition and processing of the Raman spectra were carried out using the Labspec  
121 software. For baseline correction, peak deconvolution, and spectra smoothing (using "adjacent  
122 averaging" with a step size of 40), the Origin software was employed. Values for  $R_D$  and  $S_D$   
123 (both are ratios that can be used to quantify the peak change numerically; see also further  
124 below) were calculated prior to spectra smoothing.



125  
126 *Figure 1 Experimental Setup: The saline solution was loaded into a hydrothermal*  
127 *diamond anvil cell (HDAC). Pressure control was achieved using an external inflator, and*  
128 *pressure levels were monitored via the fluorescence of ruby spheres suspended in the sample*  
129 *chamber. Raman measurements in the solution were performed at the center of the sample*  
130 *chamber by intentionally defocusing the laser spot between the surfaces of the two diamonds.*

131

### 132 3. Results

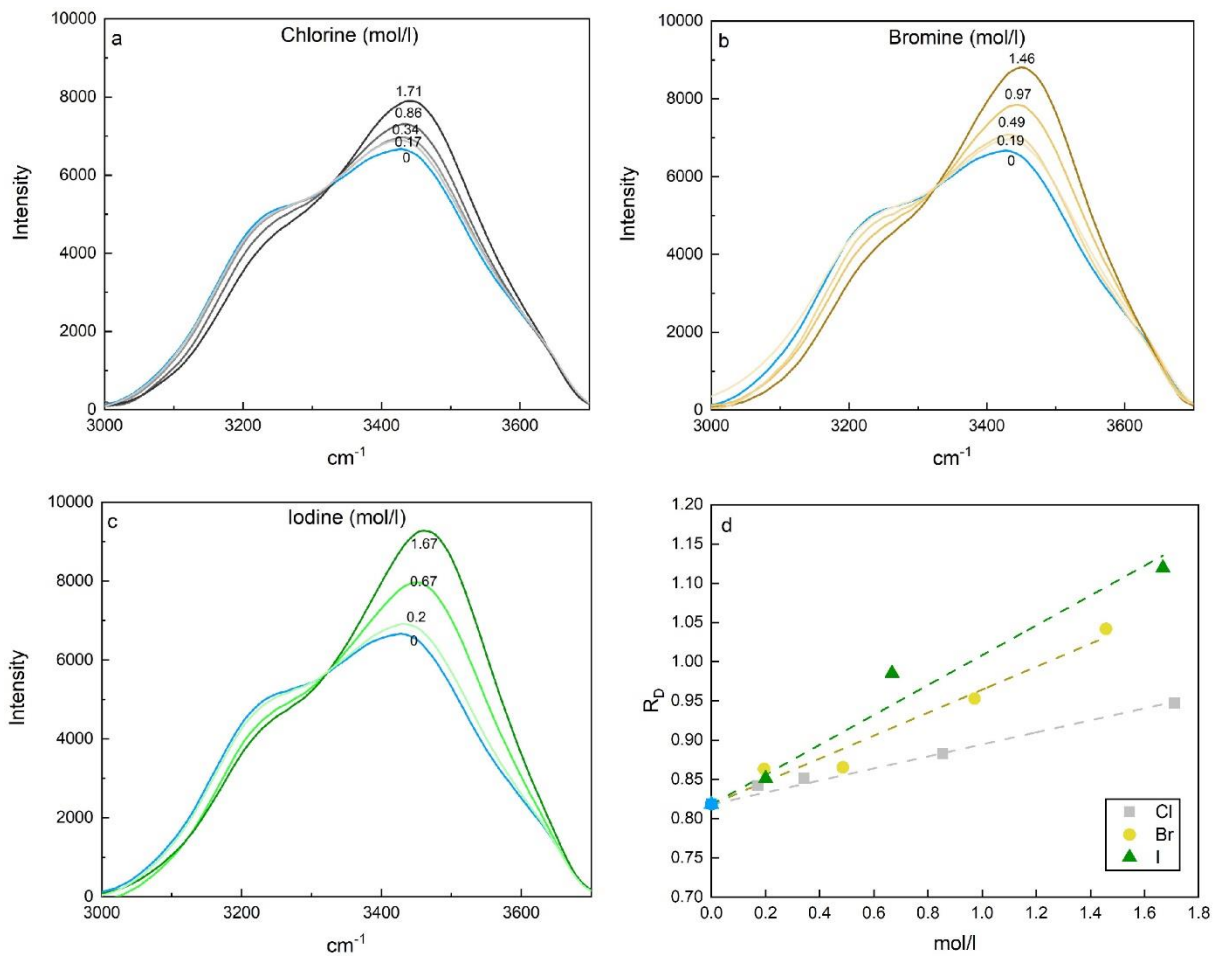
133 At ambient pressure and temperature, the configuration of the water stretching bands  
134 undergoes changes based on halogen concentration:

- 135 1. The  $3428\text{ cm}^{-1}$  peak increases with rising halogen concentration: from 6660 counts for  
136 pure water to 7900 counts for 1.71 mol/l chlorine, 8800 counts for 1.46 mol/l bromine, and  
137 9300 counts for 1.67 mol/l iodine, respectively.
- 138 2. The  $3428\text{ cm}^{-1}$  peak shifts to higher wavenumbers with specific positions at  $3441\text{ cm}^{-1}$  for  
139 chlorine,  $3450\text{ cm}^{-1}$  for bromine, and  $3460\text{ cm}^{-1}$  for iodine at their respective highest  
140 concentrations.
- 141 3. The minor peak at  $3240\text{ cm}^{-1}$  becomes relatively smaller as halogen concentration  
142 increases, decreasing from 5060 counts for water to 4400 counts for chlorine, 4190 counts  
143 for bromine, and 4430 counts for iodine (Figure 2).

144 At a constant halogen concentration, the characteristics of the water stretching bands evolve  
145 with increasing pressure:

- 146 1. The  $3428\text{ cm}^{-1}$  peak decreases with rising pressure: from 6975 counts at 0 GPa to 5960  
147 counts at 1.1 GPa for 0.34 mol/l chlorine, from 8800 counts at 0 GPa to 7350 counts at  
148 1.1 GPa for 1.45 mol/l bromine, and from 6315 counts at 0 GPa to 6010 counts at 1.39  
149 GPa for 0.2 mol/l iodine.
- 150 2. The  $3428\text{ cm}^{-1}$  peak shifts to lower wavenumbers, with new positions at  $3390\text{ cm}^{-1}$  for  
151 chlorine, from  $3450$  to  $3435\text{ cm}^{-1}$  for bromine, and from  $3430$  to  $3390\text{ cm}^{-1}$  for iodine at  
152 their respective highest pressures.
- 153 3. The minor peak at  $3240\text{ cm}^{-1}$  becomes relatively larger with increasing pressure, exhibiting  
154 a slight increase from 4970 to 5140 counts for chlorine, from 4190 to 4590 counts for  
155 bromine, and from 4960 to 5255 counts for iodine (Figure 3).





156

157 *Figure 2 The Raman water bands of saline solutions with varying concentrations of a)*  
 158 *chlorine, b) bromine, and c) iodine are depicted. The halogen concentrations are indicated on*  
 159 *the spectrum in mol/l. Notably, the resulting peak of the water bands at  $3428 \text{ cm}^{-1}$  exhibits an*  
 160 *increase and shifts further to the right with escalating halogen concentration. The Raman*  
 161 *spectrum of pure water is represented in blue. In d), there is a discernible increase in  $R_D$  with*  
 162 *escalating concentrations of chlorine, bromine, and iodine. This increase is characterized by a*  
 163 *larger sum of slopes between  $3325 \text{ cm}^{-1}$  and  $3600 \text{ cm}^{-1}$ , and a heightened peak at  $3428 \text{ cm}^{-1}$ .*  
 164 *The observed effects are smallest for chlorine and most pronounced for iodine.*

165

## 166 4. Discussion

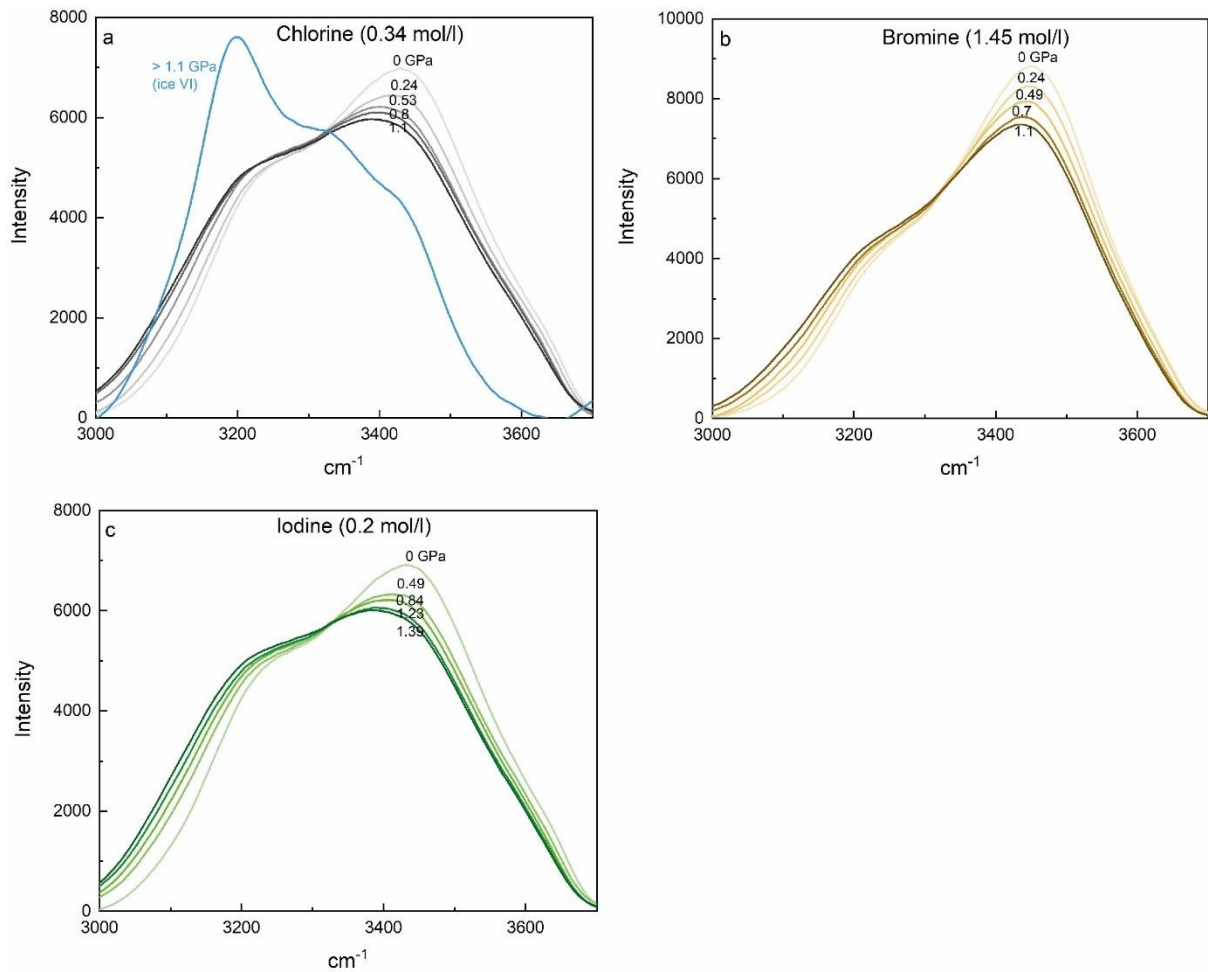
### 167 4.1. Halogen concentration and ionic size

168 The correlation between the change in the water bands' peak and varying halogen  
169 concentration, in addition to ionic size, aligns well with findings from previous studies (Dubessy  
170 et al., 2002; Durickovic et al., 2010; Georgiev et al., 1984; Mernagh and Wilde, 1989;  
171 Pankrushina et al., 2020; Sun et al., 2010; Tepstra et al., 1990). The observed shift change  
172 strength correlates directly with the ionic size of the halogens: Chlorine exhibits the smallest  
173 shift, iodine the largest, and bromine falls in between for comparable concentrations (cf.  
174 Tepstra et al., 1990 for chlorine and bromine).

175 Since ionic bonds are not Raman active, NaCl, NaBr, and NaI do not have observable modes  
176 of their own, neither as salts nor as dissolved ions in water (Bakker, 2004; Pei et al., 2006;  
177 Terpstra et al., 1990). Raman spectroscopy enables the observation of the vibration of  
178 chemical bonds, which, in this study, is the chemical vibration of water. The halogen anions  
179 are indirectly observed as they modify the vibrations of water bonding. The evolving shape of  
180 the Raman spectra in Figure 2 illustrates that different halogens influence the dominant  
181 bonding type in the water structure, leading to a reduction in hydrogen bonding in water. Figure  
182 4 presents a deconvolution of the water stretching band into three major Gaussian components  
183 representing different bonding types for water molecules:

184 Peak 1 of the first Gaussian component at  $3327\text{ cm}^{-1}$  is attributed to 4 hydrogen bonds per  
185 water molecule, involving two electron donors and two acceptors (DDAA). This peak  
186 diminishes with increasing halogen content. Peak 2 at  $3431\text{ cm}^{-1}$  is attributed to 2 hydrogen  
187 bonds (DA) and becomes the predominant bonding type with increasing halogen content. Peak  
188 3 at  $3565\text{ cm}^{-1}$  is attributed to 3 hydrogen bonds per water molecule (DDA). It plays a minor  
189 role in pure water as well as in salty solutions (e.g., Sun, 2009). With the addition of salt, the  
190 increasing presence of cations and anions breaks the hydrogen bonds in the water network,  
191 forming ionic bonds.

192 The deconvolution of the Raman water bands confirms the reduction of hydrogen bonding in  
193 water with the addition of various halogens, as well as with their increasing ionic size.



194

195 *Figure 3 The Raman water bands of saline solutions are presented with fixed halogen*  
 196 *concentrations and varying pressure: a) 0.34 mol/l chlorine, b) 1.45 mol/l bromine, and c) 0.2*  
 197 *mol/l iodine. The pressure is indicated in GPa on the spectra. Notably, the resulting peaks*  
 198 *exhibit a reduction in intensity with increasing pressure and shift towards lower wavenumbers,*  
 199 *indicating a leftward shift in the spectra.*

200

201 4.2.  $R_D$  as numerical value for the changing effect

202 To quantify the changing shift of the water stretching bands, Durickovic et al. (2010) introduced  
 203 the ratio  $S_D$ , defined by the formula:

204

$$S_D = \frac{\sum_{i=326}^{650} \left\{ \frac{I(i) + I(i-1)}{2} * [n(i) - n(i-1)] \right\}}{\sum_{i=1}^{325} \left\{ \frac{I(i) + I(i-1)}{2} * [n(i) - n(i-1)] \right\}}$$

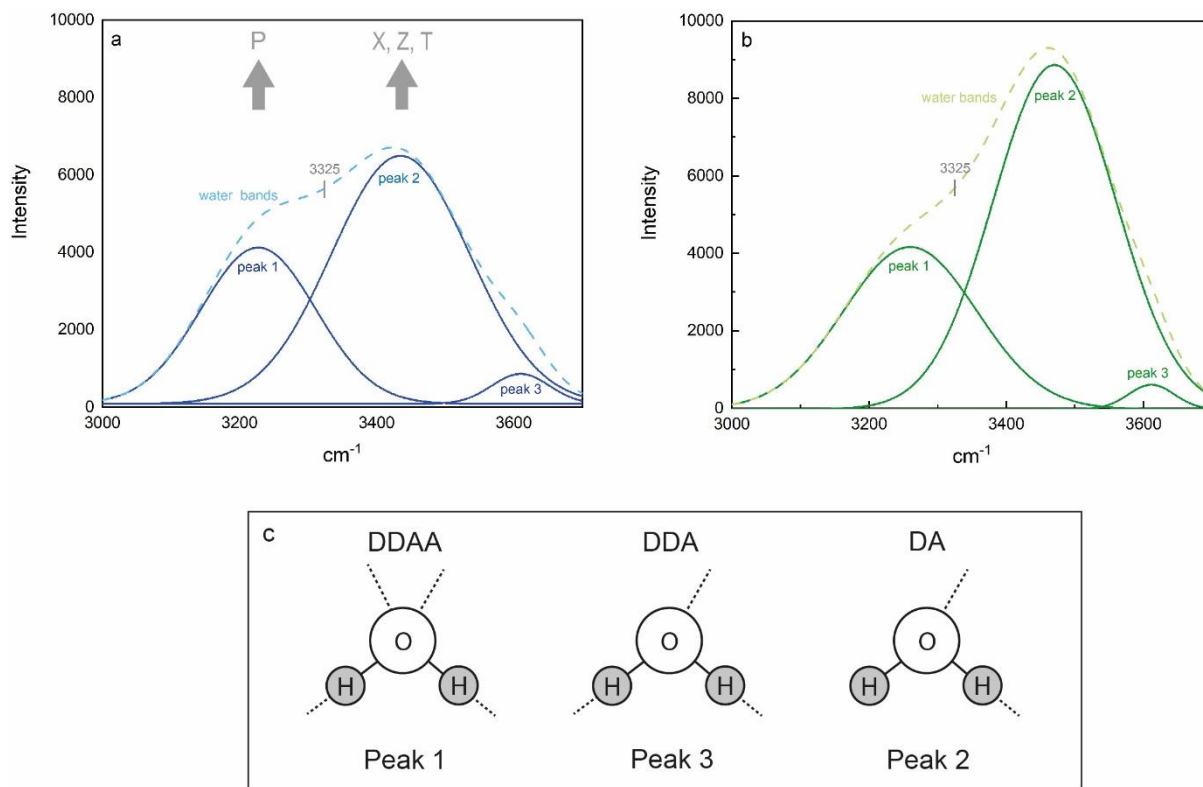
205 Here,  $n(i)$  represents the shift at increment (or pixel)  $i$ ,  $I(i)$  is the intensity at increment (or pixel)  
206  $i$ , and the range of interest is between 3000 and 3650  $\text{cm}^{-1}$  with a total of 650 pixels. This  
207 formula establishes the inflection point of the water bands at 3325  $\text{cm}^{-1}$  (Figure 4) and divides  
208 the water bands into two halves: left and right side from the inflection point. Durickovic et al.  
209 (2010) observed that  $S_D$  increases linearly with increasing NaCl concentration dissolved in  
210 water.

211 With increasing halogen concentration, the slope increases on both sides of the inflection point,  
212 resulting in an increase in both the sum of slopes for the left and right halves (cf., Figure 2).  
213 This trend holds for all three studied halogens: chlorine, bromine, and iodine. To avoid division  
214 of two values that both correlate positively and increase with higher halogen concentrations, a  
215 ratio  $R_D$  was calculated, slightly different from  $S_D$ . The formula for  $R_D$  is as follows:

$$216 \quad R_D = \frac{\sum_{i=1}^{325} \left\{ \frac{I(i) + I(i-1)}{2} * [n(i) - n(i-1)] \right\}}{I_{i=1} * 325}$$

217 Here again,  $n(i)$  represents the shift at increment (or pixel)  $i$ ,  $I(i)$  is the intensity at increment (or  
218 pixel)  $i$ , and the total number of pixels considered is 325, starting from 3325 to 3650  $\text{cm}^{-1}$ . This  
219 formula reduces some information loss from  $S_D$  and steepens the slope, as both the numerator  
220 and denominator of the ratio increase with increasing halogen concentration.

221 However, the applicability of  $R_D$  is limited to liquid water.  $R_D$  does not account for strong  
222 changes in the shape of the slope, making it less suitable for high-pressure or low-temperature  
223 polymorphs (e.g., ice VI), which exhibit the dominant peak on the left side of the inflection point  
224 (Figure 3).



225

226 *Figure 4 The peak-deconvoluted Raman water bands are presented for a) pure water*  
 227 *and b) 1.67 mol/l iodine, resolved into three Gaussian components. The resulting water bands*  
 228 *are represented by dashed lines, with the inflection point of the water bands curve identified at*  
 229 *3325 cm<sup>-1</sup>. Notably, with increasing iodine content (X) halogen ionic size (Z), and temperature*  
 230 *(T), peak 2 becomes larger relative to peak 1, while pressure (P) has the opposing effect. In*  
 231 *c), the components of the deconvolution are explained: Peak 1 is attributed to 4 hydrogen*  
 232 *bonds per water molecule, involving two electron donors and two acceptors (DDAA). Peak 2*  
 233 *is attributed to 2 hydrogen bonds (DA). Peak 3 is attributed to 3 hydrogen bonds per water*  
 234 *molecule (DDA) (Sun, 2009). The deconvolution of the Raman water bands confirms a*  
 235 *reduction in hydrogen bonding in water with the addition of various halogens and their*  
 236 *increasing ionic size. Moreover, increasing pressure correlates with an augmented number of*  
 237 *hydrogen bonds.*

238

239 4.3. Pressure

240 With increasing pressure, the water stretching band peak at  $3428\text{ cm}^{-1}$  undergoes a reduction  
241 in intensity and shifts towards the left (e.g., Romanenko et al., 2018), while the smaller peak  
242 at  $3240\text{ cm}^{-1}$  experiences a slight increase. The observed change stands in contrast to the  
243 effects observed during temperature increase (cf., Durickovic et al., 2010) or the addition of  
244 halogens (Figure 3). This shift can be interpreted as a transition towards a higher number of  
245 hydrogen bonds (from DA to DDAA) in the water molecule network (Sun, 2009, Figure 4). The  
246 effect is observable for all three halogens (chlorine, bromine, and iodine) in the saline solutions  
247 of this study (Figure 3).

248 Sun (2012) did not observe the pressure effect in their chlorine data and argue against its  
249 existence. However, upon normalizing our data in the same way as Sun (2012), the peak at  
250  $3428\text{ cm}^{-1}$  decreases, and the water bands flatten, yet a clear pressure trend remains  
251 (Supplementary Figure S1). It remains unclear why the trend was not observed in Sun (2012).

252 At pressures greater than 1 GPa and ambient temperature, water transforms into ice VI (Figure  
253 3). Notably, with increasing halogen concentrations, the water-ice phase transformation shifts  
254 to higher pressures. In this study, liquid water/saline solution was observed at 1.1 GPa and  
255 0.34 mol/l chlorine, 1.37 GPa and 0.97 mol/l bromine, or 1.27 GPa and 0.67 mol/l iodine. The  
256 experimental setup does not precisely determine if the phase boundary shifts to higher  
257 pressure or if the liquid state is metastable. Journaux et al. (2013) investigated the impact of  
258 NaCl on the phase boundary of ice VI and found the boundary at 1.01 GPa for 1 mol/l, 1.09  
259 GPa for 2.5 mol/l, and 1.52 GPa for 4 mol/l at ambient temperature. This boundary shift is  
260 much smaller than the observed range, suggesting a metastable liquid phase in our study or  
261 other kinetic effects.

262 As a consequence of the pressure-related shape change of the water stretching bands,  $R_D$   
263 decreases with increasing pressure for fixed halogen concentrations (Figure 3). Figure 5  
264 illustrates the  $R_D$  values vs. halogen concentration at different pressures ( $S_D$  values in  
265 Supplementary Figure S2). Despite some outliers, the values follow a linear trend in the studied  
266 range, as previously observed for various temperatures (Durickovic et al., 2010). Within the

267 range of comparable pressures, chlorine exhibits the lowest  $R_D$  values, while iodine  
268 demonstrates the highest. Comparable trends are also observed for integrated intensities  
269 (Supplementary Figure S3) but show larger scatter relative to the  $R_D$  trends in Figure 2d and  
270 Figure 5.

271

## 272 4.4. Applications

### 273 4.4.1. Natural fluid inclusions with one unknown component ( $P$ or $X$ )

274  $R_D$  can be calculated from Raman spectra of natural fluid inclusions in minerals, as  
275 demonstrated by Kawamoto et al. (2013). In their study, saline fluid inclusions in spinel-  
276 harzburgite xenoliths collected from the 1991 Pinatubo pumice deposits were examined. The  
277 salinity of the fluid inclusions was reported as  $5.1 \pm 1$  wt.% NaCl equivalent ( $0.87 \pm 0.17$  mol/l),  
278 measured with microthermometry. The authors employed Raman spectroscopy for qualitative  
279 water measurements.

280 From the provided Raman spectrum, a  $R_D$  value of 0.79 can be calculated. The measured  
281 chlorine concentration from microthermometry allows for an estimate of the pressure to be  
282 around 0.5 GPa (Figure 5a). This is notably lower than the 2-3 GPa that Kawamoto and  
283 colleagues estimated for the formation of the saline fluid inclusions in olivine below the  
284 Pinatubo. Given the available information, it can only be speculated whether some (parts) of  
285 the olivines formed at a very low pressure of 0.5 GPa, or if the inclusion lost pressure, and it  
286 was not fully closed above 0.5 GPa. In this case, the inclusion could at least partially represent  
287 the conditions at 0.5 GPa rather than at 2-3 GPa.

288 It is crucial to note that a fluid inclusion that closes between 810 °C and 1050 °C (Kawamoto  
289 et al., 2013) will experience a decrease in pressure when cooling down to ambient  
290 temperature. This phenomenon is also well observed in HDAC experiments (e.g., Bureau et  
291 al., 2010, 2016; Leroy et al., 2019; Louvel et al., 2020a, 2020b) and argues for a higher  
292 pressure than the 0.5 GPa that were obtained from the Raman spectrum. However, this sample

293 serves as a good illustration of how pressure can be estimated by Raman in saline fluid  
294 inclusions with given salinity.

295

#### 296 4.4.2. *Natural fluid inclusions with two unknown components (P and X)*

297 Difficulties arise when neither pressure nor salinity can be determined with a different method,  
298 and only the Raman spectrum is available. This scenario may occur for fluid inclusions that  
299 are too small for microthermometry, resulting in a single equation with two unknown  
300 parameters that cannot be solved for a distinct value.

301 Saline fluid inclusions from quartz samples analyzed by Pankrushina et al. (2020) illustrate the  
302 pressure dependence in Figure 5d, where  $R_D$  values plot as a constant line. For instance, q1  
303 has 1.9 mol/L NaCl at ambient pressure and 2.71 mol/L at 0.16 GPa; q2 has 1.88 mol/L and  
304 2.69 mol/L; and q3 has 1.02 mol/L and 1.75 mol/L at ambient pressure and at 0.16 GPa,  
305 respectively. For an unknown pressure, a single salinity value cannot be determined this way.  
306 Particularly at lower salinity concentrations, the range of possible salinities can be drastic: for  
307 the three natural samples q1-3, a small pressure increase of 0.16 GPa changes the salinity by  
308 42 to 72%. Given the stability field of quartz and saline fluids at room temperature, these are  
309 conservative calculations, and a much larger pressure range of > 1 GPa must be considered.

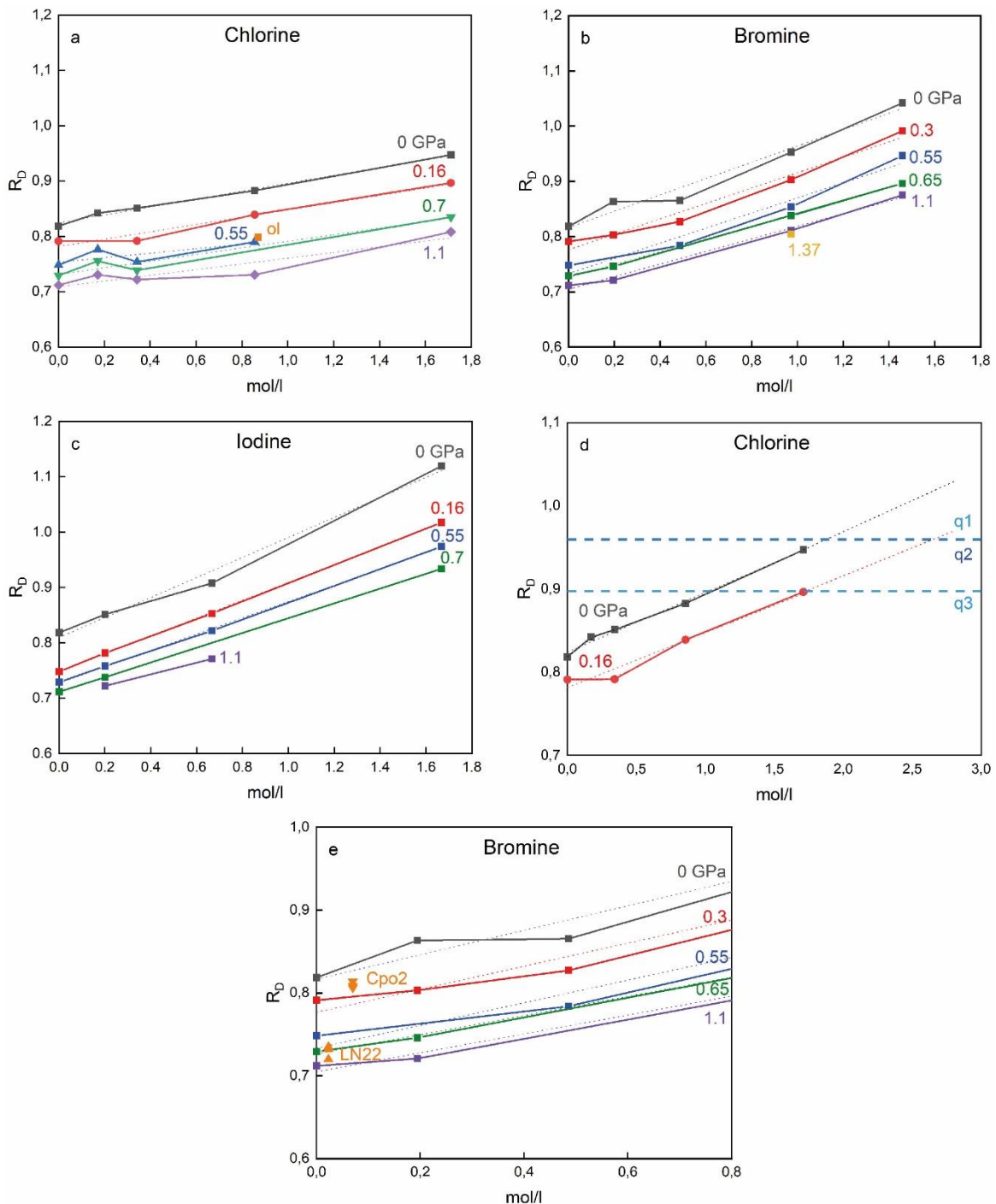
310 However, fluid inclusions can be saturated in NaCl, and halite crystals do coexist with saline  
311 fluids in the inclusion (e.g., Brooks et al., 2019). The solubility of NaCl in water at ambient P-T  
312 conditions is 317 g/l or 5.4 mol/l (cf. Figure 5). The pressure effect is diminished at NaCl-  
313 saturated conditions: Experiments in this study were conducted up to a salinity of 1.71 mol/L  
314 for NaCl, but assuming a continuation of the observed linear trend, the difference between 0  
315 and 0.16 GPa would be only 16 to 18%.

316 Therefore, the pressure effect in fluid inclusions with high salinity is smaller than in fluid  
317 inclusions with low salinity. But as the potential pressure range is large (more than 1 GPa),



318 ignoring the pressure effect can lead to a huge underestimation of the salinity in the fluid, and  
 319 Raman spectroscopy alone cannot be used to determine reliable salinities in fluid inclusions.

320



321

322 *Figure 5*  $R_D$  values vs halogen concentration for (a) chlorine, (b) bromine, and (c) iodine  
 323 are presented in the figure. The colored lines indicate isobars: the solid lines connect the data  
 324 points, while the dotted lines represent trend lines. Like the Raman water bands and the  $R_D$

325 values, the isobars exhibit the steepest slope for high concentrations of iodine and become  
326 flatter with smaller ionic halogen size, but also with increasing pressure. (a) "ol" data are from  
327 a natural fluid inclusion in olivine (Kawamoto et al., 2013). (d) Calculated  $R_D$  values for natural  
328 fluid inclusions in quartz demonstrate the pressure effect: q1 has 1.9 mol/L NaCl equivalent at  
329 ambient pressure and 2.71 mol/L at 0.16 GPa; q2 has 1.88 mol/L and 2.69 mol/L; and q3 has  
330 1.02 mol/L and 1.75 mol/L at ambient pressure and at 0.16 GPa, respectively. The fluid  
331 inclusions were analyzed by Pankrushina et al. (2020) (sample names are q1 = 672; q2 =  
332 33604; q3 = 20512). (e) Cpo2 and LN22 are experimental HDAC samples. Bromine content  
333 was analyzed with X-ray fluorescence following the methods reported in Bureau et al. (2010)  
334 and Grützner et al. (2024).

335

#### 336 4.4.3. Heavy halogens in HDAC experiments

337 The heavy halogens bromine and iodine typically play a minor role in natural fluid inclusions.  
338 The Cl/Br ratio in seawater is approximately 30, and the Cl/I ratio is around 50 (cf. Shaw and  
339 Cooper, 1957 for iodine). Due to enrichment and depletion processes in the Earth's mantle,  
340 Cl/Br ratios can vary significantly, ranging, for example, in diamond inclusions from 1 to 500  
341 (Jonson et al., 2000). Despite their low concentration and minor role in fluid inclusions, heavy  
342 halogens are highly reactive and serve as important chemical agents in Earth's atmosphere  
343 (Fehn et al., 2012). Particularly for bromine, volcanoes have been recognized as significant  
344 contributors (Gerlach et al., 2004), if not the primary controlling factor (Pyle and Mather, 2009),  
345 to the current atmospheric content. This recognition is crucial, as bromine can be  
346 approximately 60 times more efficient (Sinnhuber et al., 2009) than chlorine in the destruction  
347 of stratospheric ozone (Daniel et al., 1999; Gerlach et al., 2004).

348 Over the past few decades, numerous studies have conducted high-pressure experiments on  
349 bromine- and iodine-bearing fluids interacting with silica melts in hydrothermal diamond anvil  
350 cells (HDAC). In these studies, the halogen content in the fluid was measured using  
351 synchrotron X-ray fluorescence (Bureau et al., 2010, 2016; Kawamoto et al., 2014; Leroy et

352 al., 2019; Louvel et al., 2020a, 2020b). These experiments provide valuable insights into the  
353 behavior of heavy halogens during fluid-magma degassing processes.

354 However, these experiments entail complex setups and lack reliable and easily adaptable  
355 pressure sensors. The fluorescence wavelength shift of ruby is a commonly used pressure  
356 sensor (e.g., Chervin et al., 2001; Shen et al., 2020), but it cannot be applied in experiments  
357 conducted at elevated temperatures where ruby spheres dissolve. Other pressure indicators,  
358 like X-ray diffraction of gold particles, are only reliable at higher temperatures (cf. Grützner et  
359 al., 2024; Louvel et al., 2020b). Pressure monitoring in these HDAC experiments is essential  
360 to understand the pressure effect on halogen partitioning between silicate melts and aqueous  
361 fluids. Moreover, it is crucial to exclude pressure loss processes during the experiment (cf.  
362 Bureau et al., 2010, 2016; Leroy et al., 2019; Louvel et al., 2020a, 2020b).

363 Most HDAC experiments are conducted at high temperatures, reaching several hundred  
364 degrees Celsius (e.g., Bureau et al., 2010, 2016; Grützner et al., 2024; Leroy et al., 2019;  
365 Louvel et al., 2020a, 2020b). The elevated temperature introduces an additional variable to the  
366 shift change of the water bands, as they also change with varying temperature (Krishnamurthy  
367 et al., 1983; Ratcliffe and Irish, 1982).

368 Thus far, residual pressure can be monitored at ambient temperature, for example, before and  
369 after the experiment, once the fluid has been cooled down to room temperature. Figure 5e  
370 illustrates two samples used for test measurements, following the experimental setup and the  
371 analytical methods for bromine concentration reported in Grützner et al. (2024). These  
372 samples represent experiments that tested the degassing reaction of a bromine-doped basalt  
373 melt into an aqueous fluid. Experiments were conducted at high temperatures (above the  
374 basalt solidus) and pressures of up to 1.7 GPa in a hydrothermal diamond anvil cell (cf.  
375 Grützner et al., 2024, for a detailed description of the experiments). Bromine concentrations of  
376 0.07 mol/L for sample LN22 and 0.023 mol/L for Cpo2 were measured in the fluid by  
377 synchrotron x-ray fluorescence (SXRF) during the experiments. Raman spectra of the aqueous  
378 fluids were analyzed after the experiment under room temperature conditions. Bromine

379 concentrations from SXRF, together with the Raman spectra, allow estimating pressure ranges  
380 of 0.7 to 0.9 GPa for LN22 and 0.1 to 0.2 GPa for Cpo2. These promising results show that  
381 Raman water bands can be used as pressure or salinity indicators from room to high  
382 temperatures, providing additional pressure-concentration-related temperature calibrations  
383 are performed.

384

## 385 5. Conclusion

386 Our new experimental dataset demonstrates that the impact of halogens on the change of  
387 Raman water band shifts increases with ionic size from chlorine over bromine to iodine. To  
388 address and compare these changes, we calculated the numerical value  $R_D$ . Our experiments  
389 further show that increased pressure diminishes the impact of the halogen shift change to a  
390 different extent for each of the three halogens. This can have drastic consequences for the  
391 salinity calculation of fluid inclusions in minerals like quartz or olivine. Especially in the range  
392 of low salinity, the concentration can be strongly underestimated if the pressure effect is  
393 ignored. Either pressure or salinity needs to be determined by an independent method. For  
394 experiments performed in diamond anvil cells with halogens in aqueous fluids, the change of  
395 Raman water band shifts can be a beneficial (with some restrictions) tool to monitor the  
396 pressure at room temperature, if salinity is known, and inversely this change can be used to  
397 monitor the salinity.

398

## 399 6. Acknowledgments

400 This project was funded by the ANR Projet de Recherche Collaborative VOLC-HAL-CLIM  
401 (Volcanic Halogens: from Deep Earth to Atmospheric Impacts), ANR-18-CE01-0018 (Hélène  
402 Bureau). Tobias Grützner is grateful for the EU Marie Skłodowska-Curie Fellowship “ExCliso”  
403 (Project ID 101017762). We thank K. Béneut for his support with the Raman laser we used  
404 for our experiments at the IMPMC and Y. Guarnelli for his help with the DAC alignment. We

405 are very grateful to E.A. Pankrushina for providing the raw dataset of Raman spectra from  
406 her study. We thank the two reviewers for their helpful comments to improve the manuscript  
407 and editor Claudia Romano is thanked for handling the manuscript.

408

409

410 Statement: During the preparation of this work the authors used ChatGPT 3.5 to correct  
411 errors of spelling, punctuation, grammar and to improve the syntax in several chapters of the  
412 manuscript. After using this tool, the authors reviewed and edited the content and take full  
413 responsibility for the content of the publication.

414

415 7. References

- 416 Aiuppa, A., Baker, D.R., & Webster, J.D., 2009. Halogens in volcanic systems. *Chem. Geol.*,  
417 **263(1-4)**, 1-18. <https://doi.org/10.1016/j.chemgeo.2008.10.005>.
- 418 Bakker, R.J., 2004. Raman spectra of fluid and crystal mixtures in the systems H<sub>2</sub>O, H<sub>2</sub>O-NaCl  
419 and H<sub>2</sub>O-MgCl<sub>2</sub> at low temperatures: applications to fluid-inclusion research. *Can. Mineral.*  
420 **42**, 1283-1314. <https://doi.org/10.2113/gscanmin.42.5.1283>.
- 421 Besemer, M., Bloemenkamp, R., Ariese, F., van Manen, H.-J., 2016. Identification of multiple  
422 water-iodide species in concentrated NaI solutions based on the raman bending vibration of  
423 water. *J. Phys. Chem. A* **120(5)**, 709-714. <https://doi.org/10.1021/acs.jpca.5b10102>.
- 424 Brooks, H.L., Dragovic, B., Lamadrid, H.M., Caddick, M.J., Bodnar, R.J., 2019. Fluid capture  
425 during exhumation of subducted lithologies: A fluid inclusion study from Sifnos, Greece.  
426 *Lithos* **332-333**, 120-134. <https://doi.org/10.1016/j.lithos.2019.01.014>.
- 427 Bureau, H., Keppler, H., and Métrich, N., 2000. Volcanic degassing of bromine and iodine:  
428 Experimental fluid/melt partitioning data and applications to stratospheric chemistry: *Earth*  
429 *Planet. Sci. Lett.* **183**, 51-60. [https://doi.org/10.1016/S0012-821X\(00\)00258-2](https://doi.org/10.1016/S0012-821X(00)00258-2).
- 430 Bureau, H., Foy, E., Raepsaet, C., Somogyi, A., Munsch, P., Simon, G., Kubsy, S., 2010.  
431 Bromine cycle in subduction zones through in situ Br monitoring in diamond anvil cells.  
432 *Geochim. Cosmochim. Acta* **74**, 3839–3850. <https://doi.org/10.1016/j.gca.2010.04.001>.
- 433 Bureau, H., Auzende, A.-L., Marocchi, M., Raepsaet, C., Munsch, P., Testemale, D., Mézouar,  
434 M., Kubsy, S., Carrière, M., Ricolleau, A., Fiquet, G., 2016. Modern and past volcanic  
435 degassing of Iodine. *Geochim. Cosmochim. Acta* **173**, 114–125.  
436 <https://doi.org/10.1016/j.gca.2015.10.017>.
- 437 Chervin, J.C, Canny B., Besson, J. M., Pruzan, P., 1995. A diamond anvil cell for IR  
438 microspectroscopy. *Rev. Sci. Instrum.* **66** (3), 2595-2598. <https://doi.org/10.1063/1.1145594>.

439 Chervin J.C., Canny B., Mancinelli M., 2001. Ruby-spheres as pressure gauge for optically  
440 transparent high pressure cells. *High Press. Res.* **21**, 305–314.  
441 <https://doi.org/10.1080/08957950108202589>.

442 Daniel, J.S., Solomon, S., Portmann, R.W., 1999. Stratospheric ozone destruction: The  
443 importance of bromine relative to chlorine. *J. Geophys. Res.* **104**, 23871-23880.  
444 <https://doi.org/10.1029/1999JD900381>.

445 Dubessy J., Lhomme, T., Boiron, M-C., Rull, F., 2002. Determination of Chlorinity in Aqueous  
446 Fluids Using Raman Spectroscopy of the Stretching Band of Water at Room Temperature:  
447 Application to Fluid Inclusions. *Appl. Spectrosc.* **56(1)**, 99-106.

448 Đuričković, I., Marchetti, M., Claverie, R., Bourson, P., Chassot, J-M., Fontana, M.D., 2010.  
449 Experimental study of NaCl aqueous solutions by Raman spectroscopy: Towards a new  
450 optical sensor. *Appl. Spectrosc.* **64(8)**, 853-857.  
451 <https://doi.org/10.1366/000370210792080984>.

452 Fehn, U., 2012. Tracing crustal fluids: Applications of natural <sup>129</sup>I and <sup>36</sup>C. *Annu. Rev. Earth  
453 Planet. Sci.* **40**, 45-67. <https://doi.org/10.1146/annurev-earth-042711-105528>.

454 Georgiev, G.M., Kalkanjiev, T.K., Petrov, V.P., Nickolov, Zh., 1984. Determination of Salts in  
455 Water Solutions by a Skewing Parameter of the Water Raman Band. *Appl. Spectrosc.* **38(4)**,  
456 593-595. <https://doi.org/10.1366/0003702844555106>.

457 Gerlach, T.M., 2004. Volcanic source of tropospheric ozone-depleting trace gases. *Geochem.  
458 Geophys. Geosyst.* **5**, Q09007. <https://doi.org/10.1029/2004GC000747>.

459 Grützner, T., Bureau, H., Boulard, E., Munsch, P., Guignot, N., Siebert, J., Guarnelli, Y., 2024.  
460 An in-situ experimental HP/HT study on bromine release from a natural basalt. *Chem. Geol.*  
461 **644**, 121869. <https://doi.org/10.1016/j.chemgeo.2023.121869>.

462 Johnson, L.H., Burgess, R., Turner, G., Milledge, H.J., Harris, J.W. 2000. Noble gas and  
463 halogen geochemistry of mantle fluids: comparison of African and Canadian diamonds.  
464 *Geochim. Cosmochim. Acta* **64**, 717-732. [https://doi.org/10.1016/S0016-7037\(99\)00336-1](https://doi.org/10.1016/S0016-7037(99)00336-1).

465 Journaux, B., Daniel, I., Caracas, R., Montagnac, G., Cardon, H., 2013. Influence of NaCl on  
466 ice VI and ice VII melting curves up to 6 GPa, implications for large icy moons. *Icarus* **226**,  
467 355-363. <https://doi.org/10.1016/j.icarus.2013.05.039>.

468 Kawamoto, T., Yoshikawa, M., Kumagai, Y., Mirabueno, M.H.T., Okuno, M., Kobayashi, T.,  
469 2013. Mantle wedge infiltrated with saline fluids from dehydration and decarbonation of  
470 subducting slab. *Proc. Nat. Acad. Sci. USA.*, **110(24)**, 9663-9668.  
471 <https://doi.org/10.1073/pnas.1302040110>.

472 Kawamoto, T., Mibe, K., Bureau, H., Reguer, S., Mocuta, C., Kubsy, S., Thiaudière, D., Ono,  
473 S., Kogiso, T., 2014. Large-ion lithophile elements delivered by saline fluids to the sub-arc  
474 mantle. *Earth Planets Space* **66**, 61. <https://doi.org/10.1186/1880-5981-66-61>.

475 Krishnamurthy, S., Bansil, R., Wiafe-Akente, J., 1983. Low-frequency Raman spectrum of  
476 supercooled water. *J. Chem. Phys.* **79**, 5863-5870. <https://doi.org/10.1063/1.445756>.

477 Leroy, C.; Bureau, H., Sanloup, C., Raepsaet, C., Glazirin, K., Munsch, P., Harmand, M.,  
478 Prouteau, G., Khodja, H., 2019. Xenon and iodine behaviour in magmas. *Earth. Planet. Sci.*  
479 *Lett.* **522**, 144-154. <https://doi.org/10.1016/j.epsl.2019.06.031>.

480 Louvel, M., Cadoux, A., Brooker, R.A., Proux, O., Hazemann, J-L., 2020a. New insights on Br  
481 speciation in volcanic glasses and structural controls on halogen degassing. *Am. Min.* **105**,  
482 795-802. <https://doi.org/10.2138/am-2020-7273>.

483 Louvel, M., Sanchez-Valle, C., Malfait, W.J., Pokrovski, G.S., Borca, C.N., Grolimund, D.,  
484 2020b. Bromine speciation and partitioning in slab-derived aqueous fluids and silicate melts  
485 and implications for halogen transfer in subduction zones. *Solid Earth* **11**, 1145-1161.  
486 <https://doi.org/10.5194/se-11-1145-2020>.

487 Mernagh, T.P., Wilde, A.R., 1989. The use of the laser Raman microprobe for the  
488 determination of salinity in fluid inclusions. *Geochim. Cosmochim. Acta* **53(4)**, 765-771.  
489 [https://doi.org/10.1016/0016-7037\(89\)90022-7](https://doi.org/10.1016/0016-7037(89)90022-7).



490 Moncada, D., Bodnar, R.J., 2012. Raman spectroscopy technique to determine the salinity of  
491 fluid inclusions, PACROFI-XI (Pan-American Current Research on Fluid Inclusions)  
492 Conference, pp. 67.

493 Ni, P., Ding, J., Rao, B., 2006. In situ cryogenic Raman spectroscopic studies on the synthetic  
494 fluid inclusions in the systems H<sub>2</sub>O and NaCl-H<sub>2</sub>O. *Chin. Sci. Bull.* **51(1)**, 108-114.  
495 <https://doi.org/10.1007/s11434-004-0256-5>.

496 Pankrushina, E.A., Krupenin, M.T., Shchapova, Y.V., Kobuzov, A.S., Garaeva, A.A., Votyakov,  
497 S.L., 2020. The study of fluid inclusion salinity in minerals by raman spectroscopy revisited.  
498 In: Votykov, S., Kiseleva, D., Grokhovsky, V., Shchapova, J. (eds.), *Minerals: Structure,*  
499 *Properties, Methods of Investigation: Proceedings of the 10th All-Russian Youth Scientific*  
500 *Conference* (pp. 175-183). Springer International Publishing. <https://doi.org/10.1007/978-3->  
501 [030-49468-1\\_23](https://doi.org/10.1007/978-3-030-49468-1_23).

502 Pyle, D.M., Mather, T.A., 2009. Halogens in igneous processes and their fluxes to the  
503 atmosphere and oceans from volcanic activity: A review. *Chem. Geol.* **263**, 110-121.  
504 <https://doi.org/10.1016/j.chemgeo.2008.11.013>.

505 Ratcliffe, C.I., Irish, D.E., 1982. Vibrational spectral studies at elevated temperatures and  
506 pressures. Raman studies of liquid water up to 300 °C. *J. Phys. Chem.* **86**, 4897-4905.  
507 <https://doi.org/10.1021/j100222a013>.

508 Romanenko, A.V., Rashchenko S.V., Goryainov, S.V., Likhacheva  
509 <https://doi.org/10.1177/0003702817752487>, A.Y., Korsakov, A.V., 2018. In Situ Raman  
510 Study of Liquid Water at High Pressure. *Appl. Spectrosc.* **72(6)**, 847-852.  
511 <https://doi.org/10.1177/0003702817752487>.

512 Shaw, T., Cooper, L., 1957. State of Iodine in Sea Water. *Nature* **180**, 250.  
513 <https://doi.org/10.1038/180250a0>.

514 Shen, G., Wang, Y., Dewaele, A., Wu, C., Fratanduono, D.E., Eggert, J., Klotz, S., Dziubek,  
515 K.F., Loubeyre, P., Fat'yanov, O.V., Asimov, P.D., Mashimo, T., Wentzcovitch, R.M.M., 2020.

516 Toward an international practical pressure scale: A proposal for an IPPS ruby gauge (IPPS-  
517 Ruby2020). *High Press. Res.* **40(3)**, 299-314.  
518 <https://doi.org/10.1080/08957959.2020.1791107>.

519 Sinnhuber, B.-M., Sheode, N., Sinnhuber, M., Chipperfield, M.P., Feng, W., 2009. The  
520 contribution of anthropogenic bromine emissions to past stratospheric ozone trends: A  
521 modelling study, *Atmos. Chem. Phys.*, **9(8)**, 2863-2871. [https://doi.org/10.5194/acp-9-2863-](https://doi.org/10.5194/acp-9-2863-2009)  
522 2009.

523 Sun, Q., 2009. The Raman OH stretching bands of liquid water. *Vib. Spectrosc.* **51**, 213-217.  
524 <https://doi.org/10.1016/j.vibspec.2009.05.002>.

525 Sun, Q., 2012. Raman spectroscopic study of the effects of dissolved NaCl on water structure.  
526 *Vib. Spectrosc.* **62**, 110-114. <https://doi.org/10.1016/j.vibspec.2012.05.007>.

527 Sun, Q., Zhao, L., Li, N., Liu, J., 2010. Raman spectroscopic study for the determination of Cl-  
528 concentration (molarity scale) in aqueous solutions: Application to fluid inclusions. *Chem.*  
529 *Geol.* **272(1-4)**, 55-61. <https://doi.org/10.1016/j.chemgeo.2010.02.004>.

530 Terpstra, P., Combes, D., Zwick, A., 1990. Effect of salts on dynamics of water: A Raman  
531 spectroscopy study. *J. Chem. Phys.* **92**, 65-70. <https://doi.org/10.1063/1.458418>.

532 Walrafen, G.E., Fisher, M.R., Hokmabadi, M.S., Yang, W.-H., 1986. Temperature dependence  
533 of the low- and high-frequency Raman scattering from liquid water. *J. Chem. Phys.* **85(12)**,  
534 6970-6982. <https://doi.org/10.1063/1.451384>.

535

536

537

## 8. Tables

	NaCl				max(NaCl) <sup>a</sup>
g/l	10	20	50	100	317
mol/l	0.17	0.34	0.86	1.71	5.42
wt.%	0.99	1.96	4.76	9.09	24.07

	NaBr				max(NaBr) <sup>a</sup>
g/l	20	50	100	150	905
mol/l	0.19	0.49	0.97	1.46	8.80
wt.%	1.96	4.76	9.09	13.04	47.51

	NaI			max(NaI) <sup>a</sup>
g/l	30	100	250	1793
mol/l	0.20	0.67	1.67	11.96
wt.%	2.91	9.09	20.00	64.20

<sup>a</sup> maximum solubility in H<sub>2</sub>O at 20 °C and ambient pressure.

538

539 *Table 1 Salt concentration in the starting solutions and maximum solubility values.*

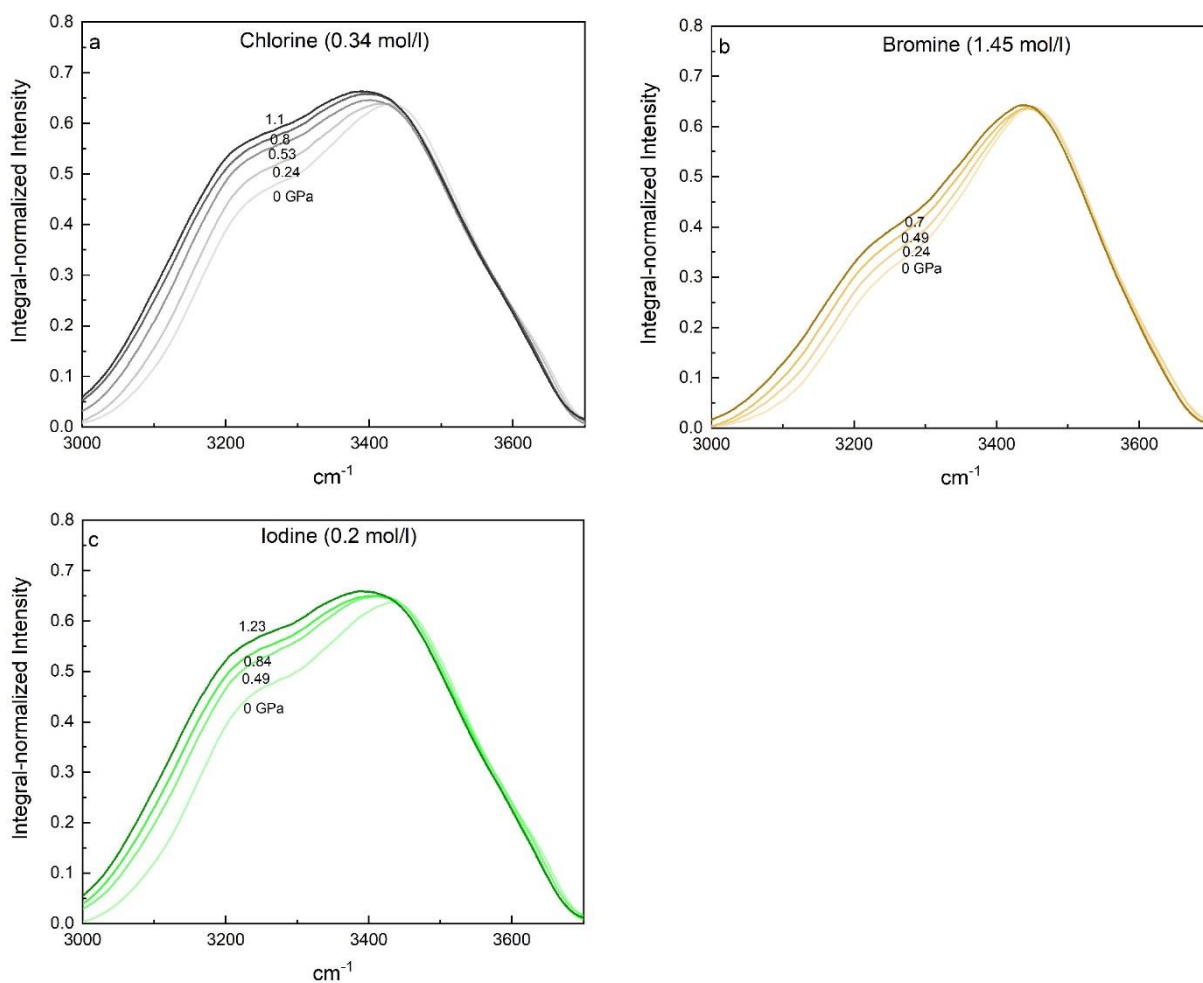
540

541

542 9. Supplementary material

543 Supplementary Tables with Raman raw data are stored under  
544 <https://data.mendeley.com/datasets/tnckfpjcv/1>.

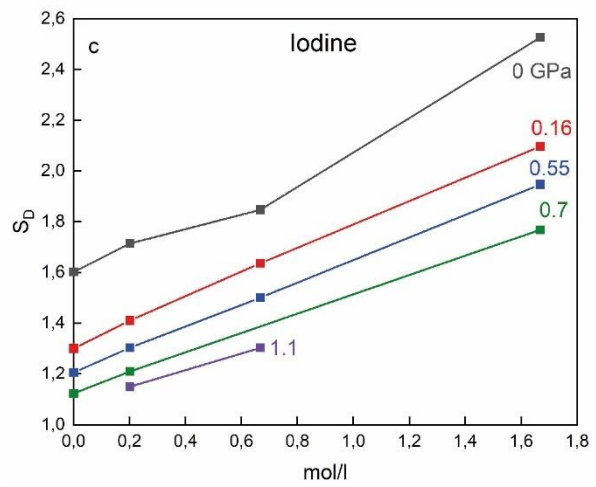
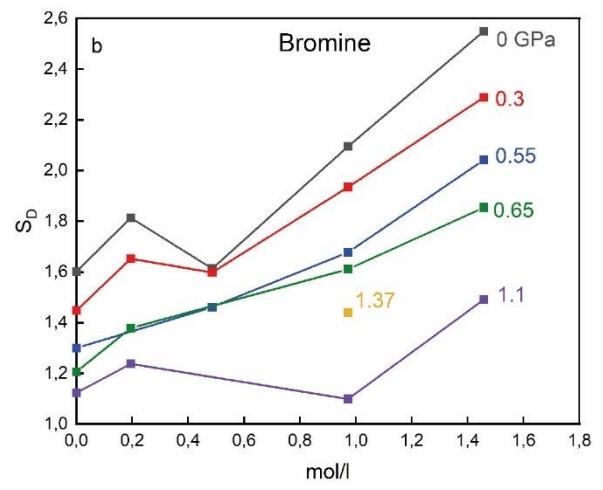
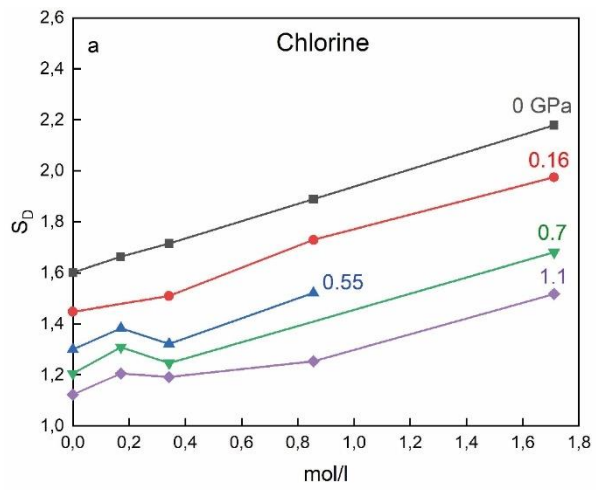
545



546

547 **Figure S1** The Raman water bands of saline solutions are presented with fixed halogen  
548 concentrations and varying pressure: a) 0.34 mol/l chlorine, b) 1.45 mol/l bromine, and c) 0.2  
549 mol/l iodine. The pressure is indicated in GPa on the spectra. Notably, the intensities are  
550 normalized to their integrated intensities for the presented range of 3000 to 3600  $\text{cm}^{-1}$ . The  
551 resulting peaks exhibit a smaller reduction than the spectra in Figure 3 but a leftward shift in  
552 the spectra indicates a clear pressure effect.

553

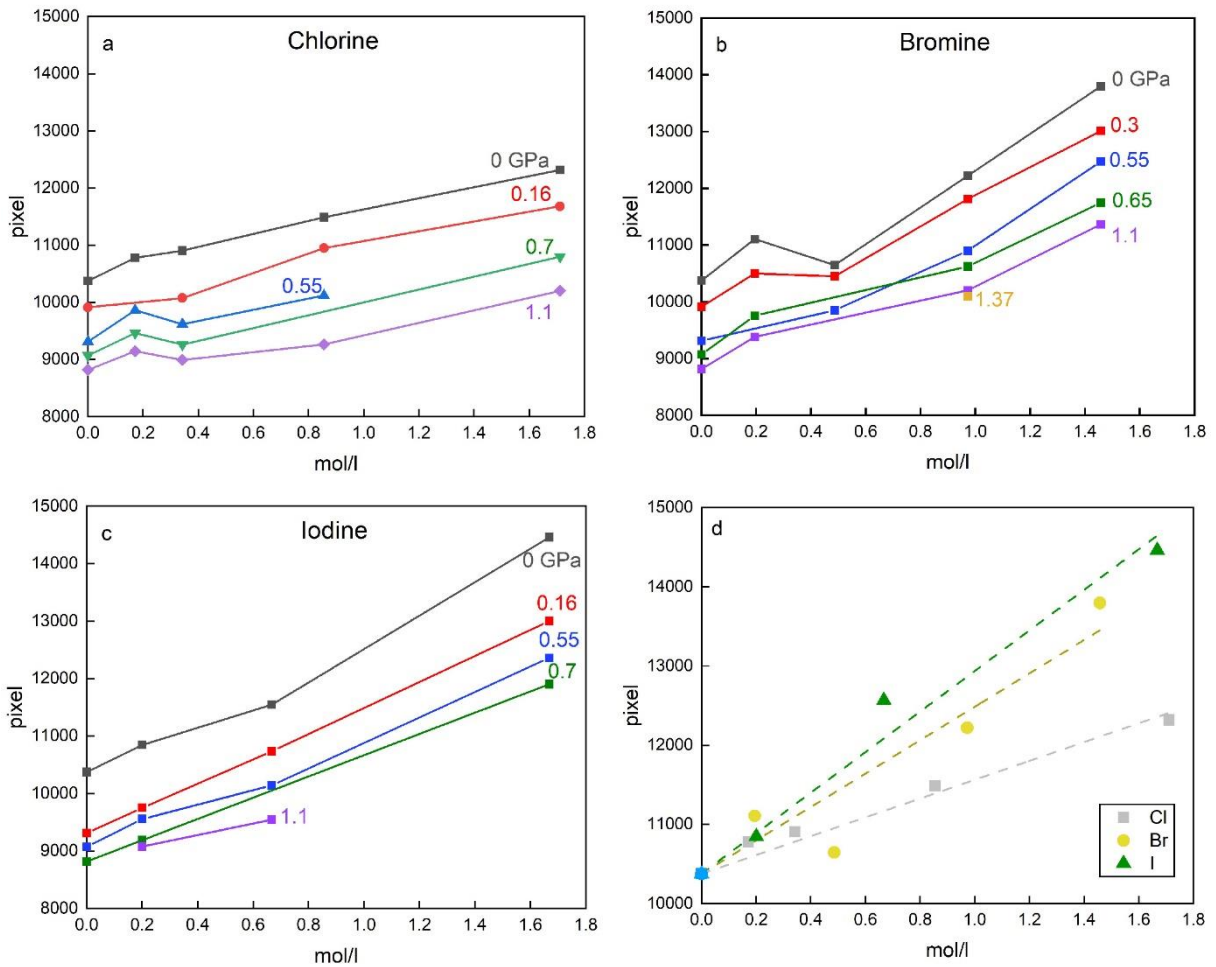


554

555 **Figure S2**  $S_D$  values vs halogen concentration for a) chlorine, b) bromine, and c) iodine

556 **calculated after Durickovic et al. (2010).**

557



558

559 **Figure S3** Integrated intensities vs halogen concentration for (a) chlorine, (b) bromine, (c)  
 560 iodine, and (d) all three elements at ambient pressure show comparable trends but large  
 561 scatter relative to the  $R_D$  values. The intensities were integrated over the range of 3000 to 3600  
 562  $cm^{-1}$ .

563

1            Heavy halogen impact on Raman water bands at high pressure:  
2                            implications for salinity estimations in fluid inclusions

3 Tobias Grützner<sup>1,2,3\*</sup>, Hélène Bureau<sup>1</sup>

4

5 <sup>1</sup> Institut de Minéralogie, de Physique des Matériaux et de Cosmochimie (IMPMC), Sorbonne  
6 Université Paris, France.

7 <sup>2</sup> Research School of Earth Sciences, Australian National University, Canberra, Australia.

8 <sup>3</sup> Institut für Geowissenschaften, Goethe-Universität Frankfurt, Germany.

9

10 \*Corresponding author

11

12 Email addresses: tobias.gruetzner@outlook.com (T. Grützner), helene.bureau@sorbonne-  
13 universite.fr (H. Bureau).

14

15

16 Abstract

17 We present a new experimental dataset on the impact of the heavy halogens chlorine, bromine  
18 and iodine on the Raman water bands concerning pressure and their concentration at room  
19 temperature. These experiments were conducted at ambient temperature, with variations in  
20 halogen concentration and pressure ranging from 0 to 1.4 GPa.

21 The strength of the Raman water band shift change increases with the ionic size from chlorine,  
22 over bromine, to iodine. Our experiments further demonstrate that increased pressure  
23 diminishes the impact of the halogen shift change to a varying extent for each of the three  
24 halogens. This finding can have significant implications for the salinity calculation of fluid  
25 inclusions in minerals such as quartz or olivine. Particularly in the low salinity range, the  
26 concentration can be markedly underestimated if the pressure effect is neglected. For  
27 experiments in diamond anvil cells involving halogens dissolved in water, the change in Raman  
28 water band shifts can serve either as a new tool to monitor pressure, or to monitor the salinity.

29

30

31 Keywords

32 Raman, water bands, Fluid inclusion, halogens, salinity, high pressure

33



34 1. Introduction

35 Halogens play a pivotal role as volatile elements, significantly impacting geodynamic  
36 processes. They constitute essential components of volcanic fumaroles and volcanic ejecta.  
37 Upon release into the atmosphere, halogens contribute to ozone destruction. In crustal  
38 hydrothermal fluids, halogen complexes (e.g., in saline fluids, brines, or molten salts) serve as  
39 major agents for metal transport in ore-forming processes related to hydrothermal systems  
40 (e.g., Aiuppa et al., 2009). Samples of such fluids can be found entrapped as inclusions in  
41 minerals like quartz (e.g., Brooks et al., 2019; Pankrushina et al., 2020) or olivine (e.g.,  
42 Kawamoto et al., 2013) in magmatic and metamorphic rocks. Raman spectroscopy has been  
43 employed for decades to determine the salinity of fluid inclusions, especially those too small  
44 for other common techniques like microthermometry – a method that determines salinity by  
45 observing and measuring the freezing temperature of the fluid (cf. e.g., Kawamoto et al., 2013;  
46 Moncada and Bodnar, 2012; Brooks et al., 2019).

47 The Raman spectra of water and aqueous fluids exhibit several peaks closely grouped at 2800-  
48 3800  $\text{cm}^{-1}$ , resulting in water stretching bands (e.g., Ratcliffe and Irish, 1982; Sun, 2009;  
49 Walrafen et al., 1986). In salty solutions or brines, halogen ions interact with the bonds of water  
50 molecules. Although ions and ionic bonding cannot be directly detected with Raman  
51 spectroscopy, their impact on the network of covalent water bonding is detectable. This effect  
52 has been the subject of numerous studies, with a substantial focus on chlorine (e.g., Dubessy  
53 et al., 2002; Durickovic et al., 2010; Georgiev et al., 1984; Mernagh and Wilde, 1989;  
54 Pankrushina et al., 2020; Sun, 2012; Sun et al., 2010; Tepstra et al., 1990) and, to a lesser  
55 extent, on the heavy halogen bromine (e.g., Tepstra et al., 1990). Halogen anions widen the  
56 water bonding network, forcing the network to change its bonding structure by favoring a  
57 certain type of bonding over others. A shift in water bands can be observed, correlating with  
58 the number of dissolved halogens and facilitating the determination of salt concentration in the  
59 solution or in mineral fluid inclusions (e.g., Dubessy et al., 2002; Durickovic et al., 2010;  
60 Georgiev et al., 1984; Mernagh and Wilde, 1989; Pankrushina et al., 2020; Sun, 2012; Sun et  
61 al., 2010; Tepstra et al., 1990).

62 The heavy halogens bromine and iodine possess a larger ionic size than chlorine. Their anions  
63 stretch the water network as much or even more than chlorine, causing a more pronounced  
64 alteration of the Raman shift (Tepstra et al., 1990). The impact of the cations (e.g., calcium,  
65 magnesium, sodium, potassium) in a salty solution seem to be negligible (Sun et al., 2010).

66 Two other factors can alter the shape of Raman water bands: (1) temperature (e.g.,  
67 Krishnamurthy et al., 1983; Ratcliffe and Irish, 1982) and (2) pressure (Romanenko et al.,  
68 2018). Increasing temperature has a similar effect to increasing halogen concentrations,  
69 enhancing the resulting peak at around  $3430\text{ cm}^{-1}$ . Pressure shifts the bands in the opposing  
70 direction: It decreases the peak at  $3430\text{ cm}^{-1}$  and increases the peak at  $3240\text{ cm}^{-1}$ .

71 While fluid inclusions in minerals are typically studied at ambient temperature and its effect  
72 can be ignored, the pressure in mineral fluid inclusions, such as those in quartz, is likely to be  
73 elevated, potentially impacting the Raman spectrum. In this study, we present a novel  
74 experimental dataset examining the impact of all three heavy halogens — chlorine, bromine,  
75 and iodine — on Raman water bands concerning pressure and halogen concentration at room  
76 temperature. We further compare our results to some natural fluid inclusion samples from other  
77 studies to demonstrate and constrain the impact of our dataset on natural fluid inclusions.

78

## 79 2. Experimental setup and methods

80 Various concentrations of NaCl, NaBr, or NaI salts were dissolved in water to synthesize salty  
81 solutions as starting materials (Table 1). Sodium-halogen salts exhibit excellent solubility in  
82 water, and sodium serves as the dominant cation in seawater-related fluids. Despite the  
83 seemingly negligible impact of cations (Sun et al., 2010), sodium was selected as the cation  
84 for all three halogens to mitigate cation effects and focus on the influence of the three halogen  
85 anions.

86 The experiments were conducted using a Chervin-type hydrothermal diamond anvil cell  
87 (HDAC) with a pressure-driving membrane (Chervin et al., 1995). The HDAC was equipped

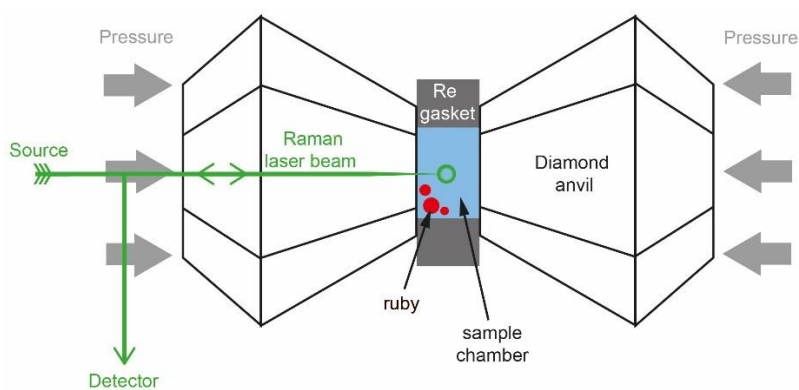
88 with 2 mm thick diamonds and culets of 1 mm diameter. The sample chamber, compressed  
89 between two diamonds, had a diameter of 500  $\mu\text{m}$ , drilled as a hole into a Re gasket with an  
90 initial thickness of 200  $\mu\text{m}$ . Before each experiment, the sample chamber was cleaned with  
91 ethanol, dried, and loaded with a salty solution along with a small number of ruby spheres for  
92 pressure calibration. Following HDAC closure, the membrane was connected to an inflator with  
93 a  $\text{N}_2$  gas bottle. The membrane was initially loaded with approximately 10 to 15 bar of gas  
94 pressure, sufficient to seal the HDAC but insufficient to observe a fluorescence shift with the  
95 ruby spheres.

96 Ruby fluorescence serves as a widely used pressure monitor for various DAC experiments  
97 (e.g., Chervin et al., 2001; Shen et al., 2020). The ruby shift was calibrated with the Raman to  
98 ambient pressure and had to be recalibrated for each new sample. After the ruby calibration,  
99 the water bands were measured with the Raman at ambient pressure. The pressure was then  
100 increased stepwise with an inflator, and pressure increases were monitored on the ruby  
101 fluorescence. Pressure steps were approximately 0.2 to 0.3 GPa. Depending on the salt  
102 concentration, the solution transforms into ice IV between 1.1 and 1.4 GPa (see below). After  
103 each pressure increase, the cell equilibrated the pressure for about 10 minutes before Raman  
104 analysis.

105 Raman measurements were performed with a 514.5 nm Argon laser and a Jobin-Yvon Horiba  
106 HR460 spectrometer. A constant grating of 1500 lines/mm, a slit size of 50  $\mu\text{m}$ , and a 50x  
107 objective placed in front of the diamond anvil cell were used. The setup was calibrated with a  
108  $521\text{ cm}^{-1}$  silicon wafer, and the laser energy was controlled to remain constant at 10 mW  
109 between each measurement during the pressure equilibration period. Diamond has no effect  
110 on the Raman water bands and is widely used for these types of studies. Test runs for pure  
111 water in the DAC and in a glass cylinder showed no difference in the spectra. Measurements  
112 in the solution were conducted in the center of the sample chamber by defocusing the laser  
113 spot between both surfaces of the two diamonds. Measurements in the solution were set for  
114 10 to 30 seconds with 3 to 5 iterations. Measurements on the ruby spheres were conducted  
115 "live" with a repetition rate of 1s.

116 It is important to note that halogens like iodine can also induce a Raman peak at around 1650  
117  $\text{cm}^{-1}$  (Besemer et al., 2016). However, this peak overlaps with the (extremely large) carbon  
118 peak from the diamond anvils and cannot be used for hydrothermal DAC experiments or for  
119 pressure calibration with HDAC.

120 The acquisition and processing of the Raman spectra were carried out using the Labspec  
121 software. For baseline correction, peak deconvolution, and spectra smoothing (using "adjacent  
122 averaging" with a step size of 40), the Origin software was employed. Values for  $R_D$  and  $S_D$   
123 (both are ratios that can be used to quantify the peak change numerically; see also further  
124 below) were calculated prior to spectra smoothing.



125  
126 *Figure 1 Experimental Setup: The saline solution was loaded into a hydrothermal*  
127 *diamond anvil cell (HDAC). Pressure control was achieved using an external inflator, and*  
128 *pressure levels were monitored via the fluorescence of ruby spheres suspended in the sample*  
129 *chamber. Raman measurements in the solution were performed at the center of the sample*  
130 *chamber by intentionally defocusing the laser spot between the surfaces of the two diamonds.*

131

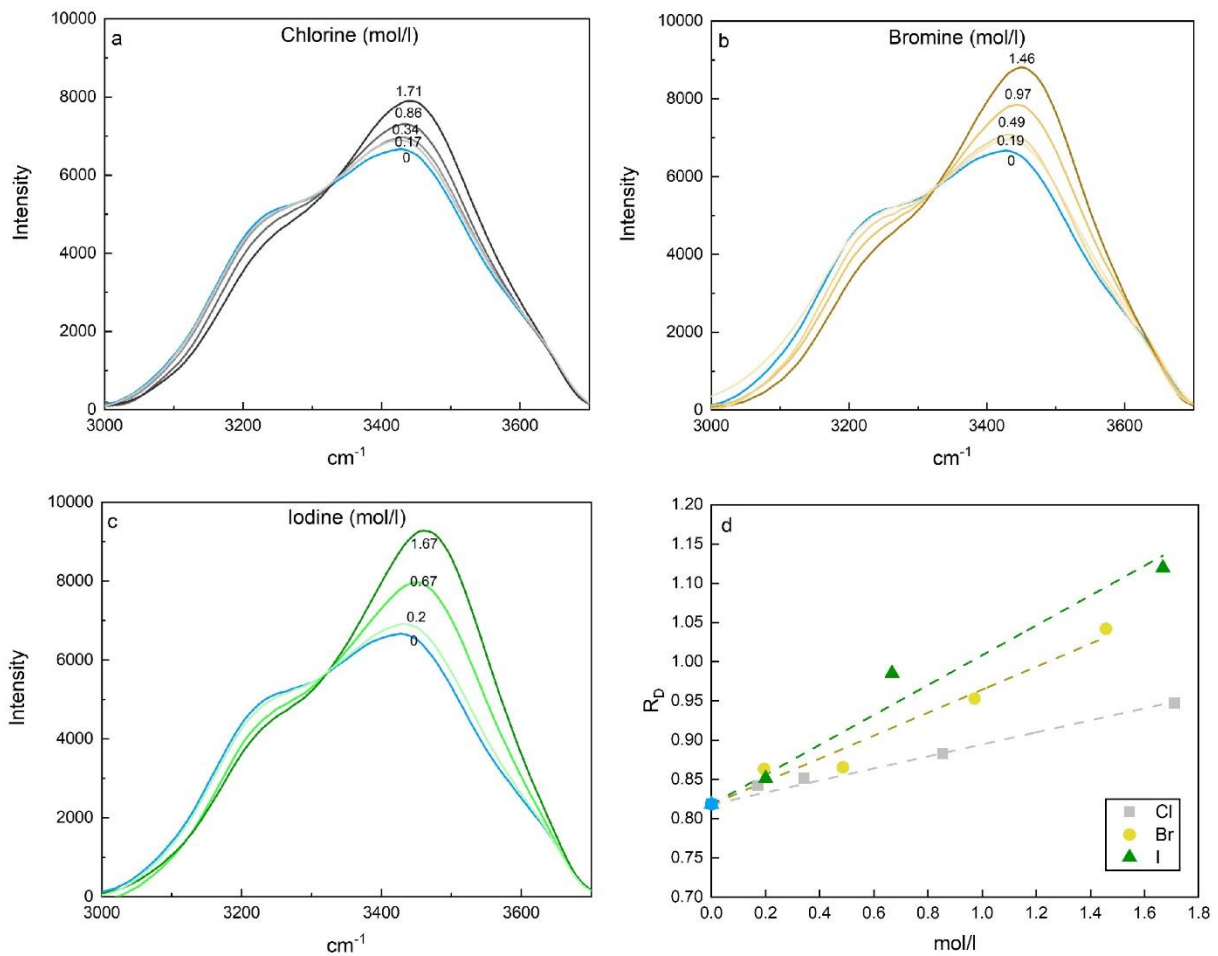
### 132 3. Results

133 At ambient pressure and temperature, the configuration of the water stretching bands  
134 undergoes changes based on halogen concentration:

- 135 1. The  $3428\text{ cm}^{-1}$  peak increases with rising halogen concentration: from 6660 counts for  
136 pure water to 7900 counts for 1.71 mol/l chlorine, 8800 counts for 1.46 mol/l bromine, and  
137 9300 counts for 1.67 mol/l iodine, respectively.
- 138 2. The  $3428\text{ cm}^{-1}$  peak shifts to higher wavenumbers with specific positions at  $3441\text{ cm}^{-1}$  for  
139 chlorine,  $3450\text{ cm}^{-1}$  for bromine, and  $3460\text{ cm}^{-1}$  for iodine at their respective highest  
140 concentrations.
- 141 3. The minor peak at  $3240\text{ cm}^{-1}$  becomes relatively smaller as halogen concentration  
142 increases, decreasing from 5060 counts for water to 4400 counts for chlorine, 4190 counts  
143 for bromine, and 4430 counts for iodine (Figure 2).

144 At a constant halogen concentration, the characteristics of the water stretching bands evolve  
145 with increasing pressure:

- 146 1. The  $3428\text{ cm}^{-1}$  peak decreases with rising pressure: from 6975 counts at 0 GPa to 5960  
147 counts at 1.1 GPa for 0.34 mol/l chlorine, from 8800 counts at 0 GPa to 7350 counts at  
148 1.1 GPa for 1.45 mol/l bromine, and from 6315 counts at 0 GPa to 6010 counts at 1.39  
149 GPa for 0.2 mol/l iodine.
- 150 2. The  $3428\text{ cm}^{-1}$  peak shifts to lower wavenumbers, with new positions at  $3390\text{ cm}^{-1}$  for  
151 chlorine, from  $3450$  to  $3435\text{ cm}^{-1}$  for bromine, and from  $3430$  to  $3390\text{ cm}^{-1}$  for iodine at  
152 their respective highest pressures.
- 153 3. The minor peak at  $3240\text{ cm}^{-1}$  becomes relatively larger with increasing pressure, exhibiting  
154 a slight increase from 4970 to 5140 counts for chlorine, from 4190 to 4590 counts for  
155 bromine, and from 4960 to 5255 counts for iodine (Figure 3).



156

157 *Figure 2 The Raman water bands of saline solutions with varying concentrations of a)*  
 158 *chlorine, b) bromine, and c) iodine are depicted. The halogen concentrations are indicated on*  
 159 *the spectrum in mol/l. Notably, the resulting peak of the water bands at 3428 cm<sup>-1</sup> exhibits an*  
 160 *increase and shifts further to the right with escalating halogen concentration. The Raman*  
 161 *spectrum of pure water is represented in blue. In d), there is a discernible increase in  $R_D$  with*  
 162 *escalating concentrations of chlorine, bromine, and iodine. This increase is characterized by a*  
 163 *larger sum of slopes between 3325 cm<sup>-1</sup> and 3600 cm<sup>-1</sup>, and a heightened peak at 3428 cm<sup>-1</sup>.*  
 164 *The observed effects are smallest for chlorine and most pronounced for iodine.*

165

## 166 4. Discussion

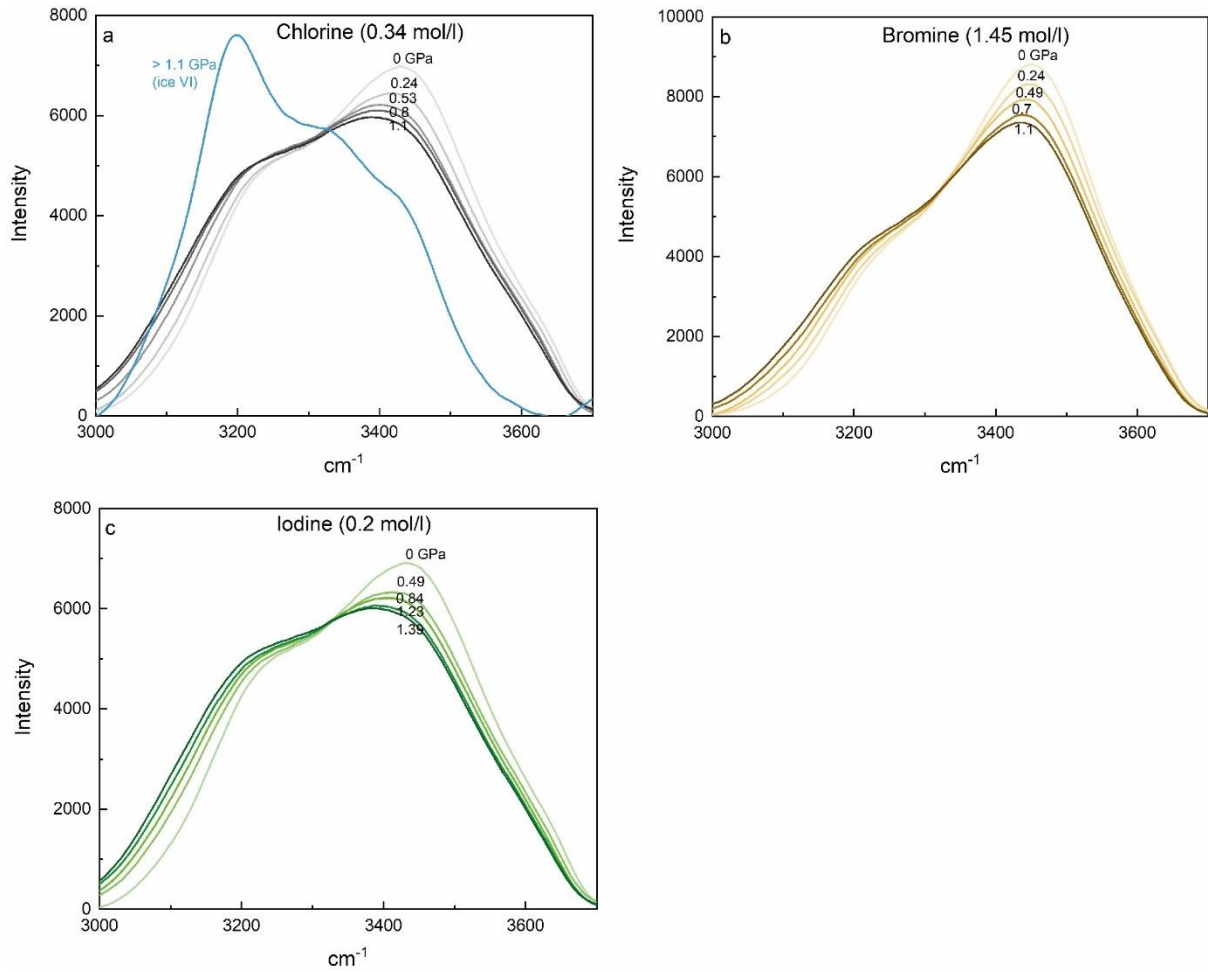
### 167 4.1. Halogen concentration and ionic size

168 The correlation between the change in the water bands' peak and varying halogen  
169 concentration, in addition to ionic size, aligns well with findings from previous studies (Dubessy  
170 et al., 2002; Durickovic et al., 2010; Georgiev et al., 1984; Mernagh and Wilde, 1989;  
171 Pankrushina et al., 2020; Sun et al., 2010; Tepstra et al., 1990). The observed shift change  
172 strength correlates directly with the ionic size of the halogens: Chlorine exhibits the smallest  
173 shift, iodine the largest, and bromine falls in between for comparable concentrations (cf.  
174 Tepstra et al., 1990 for chlorine and bromine).

175 Since ionic bonds are not Raman active, NaCl, NaBr, and NaI do not have observable modes  
176 of their own, neither as salts nor as dissolved ions in water (Bakker, 2004; Pei et al., 2006;  
177 Terpstra et al., 1990). Raman spectroscopy enables the observation of the vibration of  
178 chemical bonds, which, in this study, is the chemical vibration of water. The halogen anions  
179 are indirectly observed as they modify the vibrations of water bonding. The evolving shape of  
180 the Raman spectra in Figure 2 illustrates that different halogens influence the dominant  
181 bonding type in the water structure, leading to a reduction in hydrogen bonding in water. Figure  
182 4 presents a deconvolution of the water stretching band into three major Gaussian components  
183 representing different bonding types for water molecules:

184 Peak 1 of the first Gaussian component at  $3327\text{ cm}^{-1}$  is attributed to 4 hydrogen bonds per  
185 water molecule, involving two electron donors and two acceptors (DDAA). This peak  
186 diminishes with increasing halogen content. Peak 2 at  $3431\text{ cm}^{-1}$  is attributed to 2 hydrogen  
187 bonds (DA) and becomes the predominant bonding type with increasing halogen content. Peak  
188 3 at  $3565\text{ cm}^{-1}$  is attributed to 3 hydrogen bonds per water molecule (DDA). It plays a minor  
189 role in pure water as well as in salty solutions (e.g., Sun, 2009). With the addition of salt, the  
190 increasing presence of cations and anions breaks the hydrogen bonds in the water network,  
191 forming ionic bonds.

192 The deconvolution of the Raman water bands confirms the reduction of hydrogen bonding in  
193 water with the addition of various halogens, as well as with their increasing ionic size.



194

195 *Figure 3 The Raman water bands of saline solutions are presented with fixed halogen*  
 196 *concentrations and varying pressure: a) 0.34 mol/l chlorine, b) 1.45 mol/l bromine, and c) 0.2*  
 197 *mol/l iodine. The pressure is indicated in GPa on the spectra. Notably, the resulting peaks*  
 198 *exhibit a reduction in intensity with increasing pressure and shift towards lower wavenumbers,*  
 199 *indicating a leftward shift in the spectra.*

200

201 4.2.  $R_D$  as numerical value for the changing effect

202 To quantify the changing shift of the water stretching bands, Durickovic et al. (2010) introduced  
 203 the ratio  $S_D$ , defined by the formula:

204

$$S_D = \frac{\sum_{i=326}^{650} \left\{ \frac{I(i) + I(i-1)}{2} * [n(i) - n(i-1)] \right\}}{\sum_{i=1}^{325} \left\{ \frac{I(i) + I(i-1)}{2} * [n(i) - n(i-1)] \right\}}$$



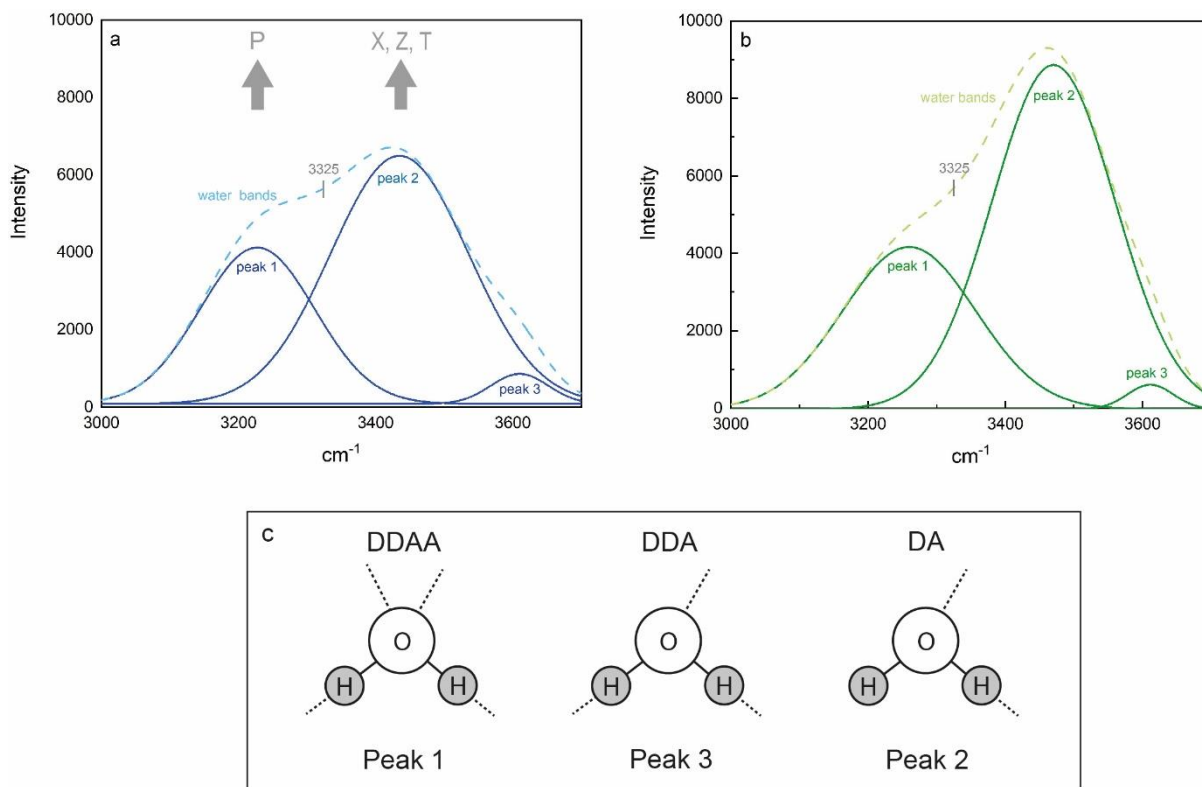
205 Here,  $n(i)$  represents the shift at increment (or pixel)  $i$ ,  $I(i)$  is the intensity at increment (or pixel)  
206  $i$ , and the range of interest is between 3000 and 3650  $\text{cm}^{-1}$  with a total of 650 pixels. This  
207 formula establishes the inflection point of the water bands at 3325  $\text{cm}^{-1}$  (Figure 4) and divides  
208 the water bands into two halves: left and right side from the inflection point. Durickovic et al.  
209 (2010) observed that  $S_D$  increases linearly with increasing NaCl concentration dissolved in  
210 water.

211 With increasing halogen concentration, the slope increases on both sides of the inflection point,  
212 resulting in an increase in both the sum of slopes for the left and right halves (cf., Figure 2).  
213 This trend holds for all three studied halogens: chlorine, bromine, and iodine. To avoid division  
214 of two values that both correlate positively and increase with higher halogen concentrations, a  
215 ratio  $R_D$  was calculated, slightly different from  $S_D$ . The formula for  $R_D$  is as follows:

$$216 \quad R_D = \frac{\sum_{i=1}^{325} \left\{ \frac{I(i) + I(i-1)}{2} * [n(i) - n(i-1)] \right\}}{I_{i=1} * 325}$$

217 Here again,  $n(i)$  represents the shift at increment (or pixel)  $i$ ,  $I(i)$  is the intensity at increment (or  
218 pixel)  $i$ , and the total number of pixels considered is 325, starting from 3325 to 3650  $\text{cm}^{-1}$ . This  
219 formula reduces some information loss from  $S_D$  and steepens the slope, as both the numerator  
220 and denominator of the ratio increase with increasing halogen concentration.

221 However, the applicability of  $R_D$  is limited to liquid water.  $R_D$  does not account for strong  
222 changes in the shape of the slope, making it less suitable for high-pressure or low-temperature  
223 polymorphs (e.g., ice VI), which exhibit the dominant peak on the left side of the inflection point  
224 (Figure 3).



225

226 *Figure 4 The peak-deconvoluted Raman water bands are presented for a) pure water*  
 227 *and b) 1.67 mol/l iodine, resolved into three Gaussian components. The resulting water bands*  
 228 *are represented by dashed lines, with the inflection point of the water bands curve identified at*  
 229 *3325 cm<sup>-1</sup>. Notably, with increasing iodine content (X) halogen ionic size (Z), and temperature*  
 230 *(T), peak 2 becomes larger relative to peak 1, while pressure (P) has the opposing effect. In*  
 231 *c), the components of the deconvolution are explained: Peak 1 is attributed to 4 hydrogen*  
 232 *bonds per water molecule, involving two electron donors and two acceptors (DDAA). Peak 2*  
 233 *is attributed to 2 hydrogen bonds (DA). Peak 3 is attributed to 3 hydrogen bonds per water*  
 234 *molecule (DDA) (Sun, 2009). The deconvolution of the Raman water bands confirms a*  
 235 *reduction in hydrogen bonding in water with the addition of various halogens and their*  
 236 *increasing ionic size. Moreover, increasing pressure correlates with an augmented number of*  
 237 *hydrogen bonds.*

238

239 4.3. Pressure

240 With increasing pressure, the water stretching band peak at  $3428\text{ cm}^{-1}$  undergoes a reduction  
241 in intensity and shifts towards the left (e.g., Romanenko et al., 2018), while the smaller peak  
242 at  $3240\text{ cm}^{-1}$  experiences a slight increase. The observed change stands in contrast to the  
243 effects observed during temperature increase (cf., Durickovic et al., 2010) or the addition of  
244 halogens (Figure 3). This shift can be interpreted as a transition towards a higher number of  
245 hydrogen bonds (from DA to DDAA) in the water molecule network (Sun, 2009, Figure 4). The  
246 effect is observable for all three halogens (chlorine, bromine, and iodine) in the saline solutions  
247 of this study (Figure 3).

248 Sun (2012) did not observe the pressure effect in their chlorine data and argue against its  
249 existence. However, upon normalizing our data in the same way as Sun (2012), the peak at  
250  $3428\text{ cm}^{-1}$  decreases, and the water bands flatten, yet a clear pressure trend remains  
251 (Supplementary Figure S1). It remains unclear why the trend was not observed in Sun (2012).

252 At pressures greater than 1 GPa and ambient temperature, water transforms into ice VI (Figure  
253 3). Notably, with increasing halogen concentrations, the water-ice phase transformation shifts  
254 to higher pressures. In this study, liquid water/saline solution was observed at 1.1 GPa and  
255 0.34 mol/l chlorine, 1.37 GPa and 0.97 mol/l bromine, or 1.27 GPa and 0.67 mol/l iodine. The  
256 experimental setup does not precisely determine if the phase boundary shifts to higher  
257 pressure or if the liquid state is metastable. Journaux et al. (2013) investigated the impact of  
258 NaCl on the phase boundary of ice VI and found the boundary at 1.01 GPa for 1 mol/l, 1.09  
259 GPa for 2.5 mol/l, and 1.52 GPa for 4 mol/l at ambient temperature. This boundary shift is  
260 much smaller than the observed range, suggesting a metastable liquid phase in our study or  
261 other kinetic effects.

262 As a consequence of the pressure-related shape change of the water stretching bands,  $R_D$   
263 decreases with increasing pressure for fixed halogen concentrations (Figure 3). Figure 5  
264 illustrates the  $R_D$  values vs. halogen concentration at different pressures ( $S_D$  values in  
265 Supplementary Figure S2). Despite some outliers, the values follow a linear trend in the studied  
266 range, as previously observed for various temperatures (Durickovic et al., 2010). Within the

267 range of comparable pressures, chlorine exhibits the lowest  $R_D$  values, while iodine  
268 demonstrates the highest. Comparable trends are also observed for integrated intensities  
269 (Supplementary Figure S3) but show larger scatter relative to the  $R_D$  trends in Figure 2d and  
270 Figure 5.

271

## 272 4.4. Applications

### 273 4.4.1. *Natural fluid inclusions with one unknown component (P or X)*

274  $R_D$  can be calculated from Raman spectra of natural fluid inclusions in minerals, as  
275 demonstrated by Kawamoto et al. (2013). In their study, saline fluid inclusions in spinel-  
276 harzburgite xenoliths collected from the 1991 Pinatubo pumice deposits were examined. The  
277 salinity of the fluid inclusions was reported as  $5.1 \pm 1$  wt.% NaCl equivalent ( $0.87 \pm 0.17$  mol/l),  
278 measured with microthermometry. The authors employed Raman spectroscopy for qualitative  
279 water measurements.

280 From the provided Raman spectrum, a  $R_D$  value of 0.79 can be calculated. The measured  
281 chlorine concentration from microthermometry allows for an estimate of the pressure to be  
282 around 0.5 GPa (Figure 5a). This is notably lower than the 2-3 GPa that Kawamoto and  
283 colleagues estimated for the formation of the saline fluid inclusions in olivine below the  
284 Pinatubo. Given the available information, it can only be speculated whether some (parts) of  
285 the olivines formed at a very low pressure of 0.5 GPa, or if the inclusion lost pressure, and it  
286 was not fully closed above 0.5 GPa. In this case, the inclusion could at least partially represent  
287 the conditions at 0.5 GPa rather than at 2-3 GPa.

288 It is crucial to note that a fluid inclusion that closes between 810 °C and 1050 °C (Kawamoto  
289 et al., 2013) will experience a decrease in pressure when cooling down to ambient  
290 temperature. This phenomenon is also well observed in HDAC experiments (e.g., Bureau et  
291 al., 2010, 2016; Leroy et al., 2019; Louvel et al., 2020a, 2020b) and argues for a higher  
292 pressure than the 0.5 GPa that were obtained from the Raman spectrum. However, this sample

293 serves as a good illustration of how pressure can be estimated by Raman in saline fluid  
294 inclusions with given salinity.

295

#### 296 4.4.2. *Natural fluid inclusions with two unknown components (P and X)*

297 Difficulties arise when neither pressure nor salinity can be determined with a different method,  
298 and only the Raman spectrum is available. This scenario may occur for fluid inclusions that  
299 are too small for microthermometry, resulting in a single equation with two unknown  
300 parameters that cannot be solved for a distinct value.

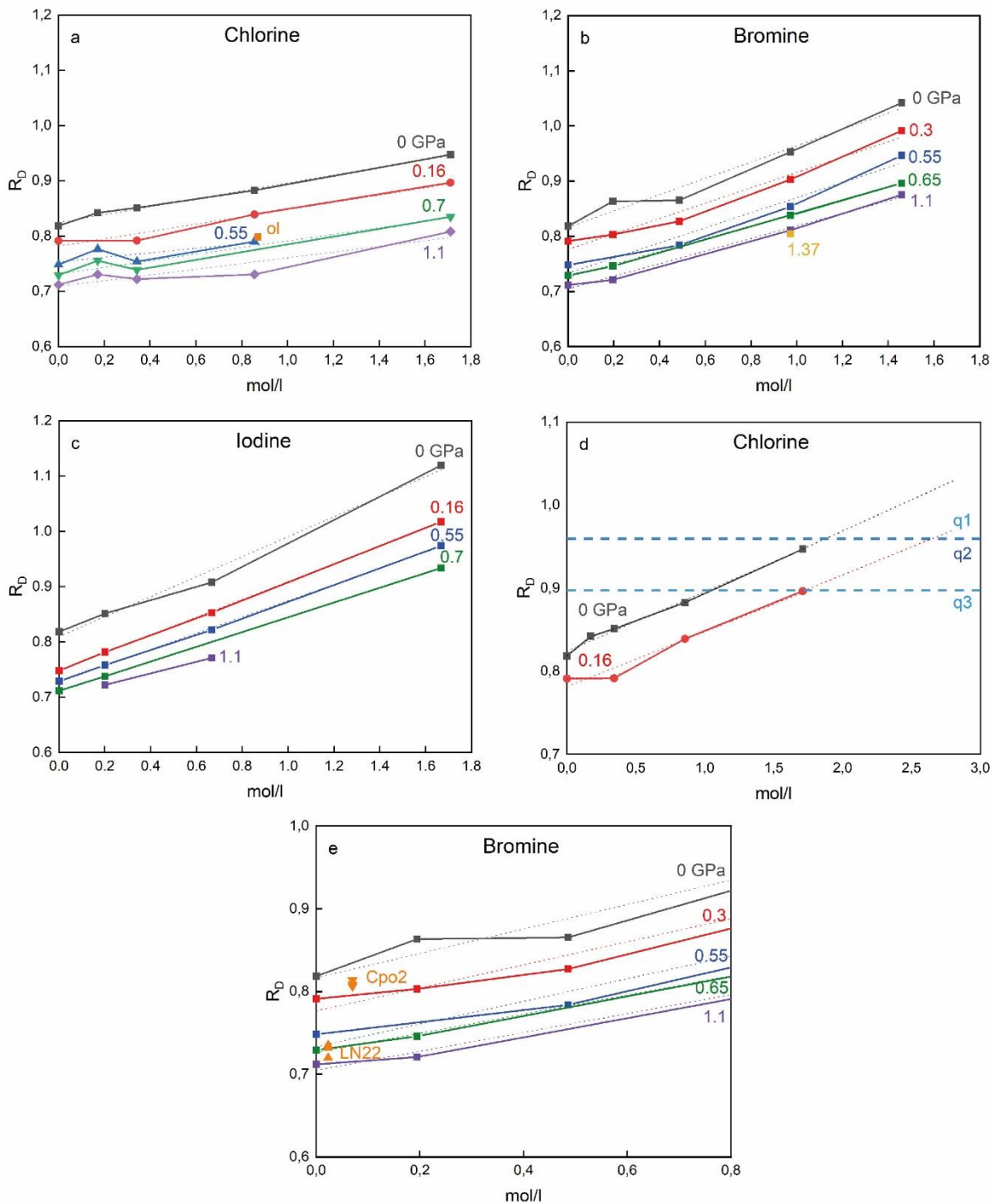
301 Saline fluid inclusions from quartz samples analyzed by Pankrushina et al. (2020) illustrate the  
302 pressure dependence in Figure 5d, where  $R_D$  values plot as a constant line. For instance, q1  
303 has 1.9 mol/L NaCl at ambient pressure and 2.71 mol/L at 0.16 GPa; q2 has 1.88 mol/L and  
304 2.69 mol/L; and q3 has 1.02 mol/L and 1.75 mol/L at ambient pressure and at 0.16 GPa,  
305 respectively. For an unknown pressure, a single salinity value cannot be determined this way.  
306 Particularly at lower salinity concentrations, the range of possible salinities can be drastic: for  
307 the three natural samples q1-3, a small pressure increase of 0.16 GPa changes the salinity by  
308 42 to 72%. Given the stability field of quartz and saline fluids at room temperature, these are  
309 conservative calculations, and a much larger pressure range of > 1 GPa must be considered.

310 However, fluid inclusions can be saturated in NaCl, and halite crystals do coexist with saline  
311 fluids in the inclusion (e.g., Brooks et al., 2019). The solubility of NaCl in water at ambient P-T  
312 conditions is 317 g/l or 5.4 mol/l (cf. Figure 5). The pressure effect is diminished at NaCl-  
313 saturated conditions: Experiments in this study were conducted up to a salinity of 1.71 mol/L  
314 for NaCl, but assuming a continuation of the observed linear trend, the difference between 0  
315 and 0.16 GPa would be only 16 to 18%.

316 Therefore, the pressure effect in fluid inclusions with high salinity is smaller than in fluid  
317 inclusions with low salinity. But as the potential pressure range is large (more than 1 GPa),

318 ignoring the pressure effect can lead to a huge underestimation of the salinity in the fluid, and  
 319 Raman spectroscopy alone cannot be used to determine reliable salinities in fluid inclusions.

320



321

322 *Figure 5*  $R_D$  values vs halogen concentration for (a) chlorine, (b) bromine, and (c) iodine  
 323 are presented in the figure. The colored lines indicate isobars: the solid lines connect the data  
 324 points, while the dotted lines represent trend lines. Like the Raman water bands and the  $R_D$

325 values, the isobars exhibit the steepest slope for high concentrations of iodine and become  
326 flatter with smaller ionic halogen size, but also with increasing pressure. (a) "ol" data are from  
327 a natural fluid inclusion in olivine (Kawamoto et al., 2013). (d) Calculated  $R_D$  values for natural  
328 fluid inclusions in quartz demonstrate the pressure effect: q1 has 1.9 mol/L NaCl equivalent at  
329 ambient pressure and 2.71 mol/L at 0.16 GPa; q2 has 1.88 mol/L and 2.69 mol/L; and q3 has  
330 1.02 mol/L and 1.75 mol/L at ambient pressure and at 0.16 GPa, respectively. The fluid  
331 inclusions were analyzed by Pankrushina et al. (2020) (sample names are q1 = 672; q2 =  
332 33604; q3 = 20512). (e) Cpo2 and LN22 are experimental HDAC samples. Bromine content  
333 was analyzed with X-ray fluorescence following the methods reported in Bureau et al. (2010)  
334 and Grützner et al. (2024).

335

#### 336 4.4.3. Heavy halogens in HDAC experiments

337 The heavy halogens bromine and iodine typically play a minor role in natural fluid inclusions.  
338 The Cl/Br ratio in seawater is approximately 30, and the Cl/I ratio is around 50 (cf. Shaw and  
339 Cooper, 1957 for iodine). Due to enrichment and depletion processes in the Earth's mantle,  
340 Cl/Br ratios can vary significantly, ranging, for example, in diamond inclusions from 1 to 500  
341 (Jonson et al., 2000). Despite their low concentration and minor role in fluid inclusions, heavy  
342 halogens are highly reactive and serve as important chemical agents in Earth's atmosphere  
343 (Fehn et al., 2012). Particularly for bromine, volcanoes have been recognized as significant  
344 contributors (Gerlach et al., 2004), if not the primary controlling factor (Pyle and Mather, 2009),  
345 to the current atmospheric content. This recognition is crucial, as bromine can be  
346 approximately 60 times more efficient (Sinnhuber et al., 2009) than chlorine in the destruction  
347 of stratospheric ozone (Daniel et al., 1999; Gerlach et al., 2004).

348 Over the past few decades, numerous studies have conducted high-pressure experiments on  
349 bromine- and iodine-bearing fluids interacting with silica melts in hydrothermal diamond anvil  
350 cells (HDAC). In these studies, the halogen content in the fluid was measured using  
351 synchrotron X-ray fluorescence (Bureau et al., 2010, 2016; Kawamoto et al., 2014; Leroy et

352 al., 2019; Louvel et al., 2020a, 2020b). These experiments provide valuable insights into the  
353 behavior of heavy halogens during fluid-magma degassing processes.

354 However, these experiments entail complex setups and lack reliable and easily adaptable  
355 pressure sensors. The fluorescence wavelength shift of ruby is a commonly used pressure  
356 sensor (e.g., Chervin et al., 2001; Shen et al., 2020), but it cannot be applied in experiments  
357 conducted at elevated temperatures where ruby spheres dissolve. Other pressure indicators,  
358 like X-ray diffraction of gold particles, are only reliable at higher temperatures (cf. Grützner et  
359 al., 2024; Louvel et al., 2020b). Pressure monitoring in these HDAC experiments is essential  
360 to understand the pressure effect on halogen partitioning between silicate melts and aqueous  
361 fluids. Moreover, it is crucial to exclude pressure loss processes during the experiment (cf.  
362 Bureau et al., 2010, 2016; Leroy et al., 2019; Louvel et al., 2020a, 2020b).

363 Most HDAC experiments are conducted at high temperatures, reaching several hundred  
364 degrees Celsius (e.g., Bureau et al., 2010, 2016; Grützner et al., 2024; Leroy et al., 2019;  
365 Louvel et al., 2020a, 2020b). The elevated temperature introduces an additional variable to the  
366 shift change of the water bands, as they also change with varying temperature (Krishnamurthy  
367 et al., 1983; Ratcliffe and Irish, 1982).

368 Thus far, residual pressure can be monitored at ambient temperature, for example, before and  
369 after the experiment, once the fluid has been cooled down to room temperature. Figure 5e  
370 illustrates two samples used for test measurements, following the experimental setup and the  
371 analytical methods for bromine concentration reported in Grützner et al. (2024). These  
372 samples represent experiments that tested the degassing reaction of a bromine-doped basalt  
373 melt into an aqueous fluid. Experiments were conducted at high temperatures (above the  
374 basalt solidus) and pressures of up to 1.7 GPa in a hydrothermal diamond anvil cell (cf.  
375 Grützner et al., 2024, for a detailed description of the experiments). Bromine concentrations of  
376 0.07 mol/L for sample LN22 and 0.023 mol/L for Cpo2 were measured in the fluid by  
377 synchrotron x-ray fluorescence (SXRF) during the experiments. Raman spectra of the aqueous  
378 fluids were analyzed after the experiment under room temperature conditions. Bromine



379 concentrations from SXRF, together with the Raman spectra, allow estimating pressure ranges  
380 of 0.7 to 0.9 GPa for LN22 and 0.1 to 0.2 GPa for Cpo2. These promising results show that  
381 Raman water bands can be used as pressure or salinity indicators from room to high  
382 temperatures, providing additional pressure-concentration-related temperature calibrations  
383 are performed.

384

## 385 5. Conclusion

386 Our new experimental dataset demonstrates that the impact of halogens on the change of  
387 Raman water band shifts increases with ionic size from chlorine over bromine to iodine. To  
388 address and compare these changes, we calculated the numerical value  $R_D$ . Our experiments  
389 further show that increased pressure diminishes the impact of the halogen shift change to a  
390 different extent for each of the three halogens. This can have drastic consequences for the  
391 salinity calculation of fluid inclusions in minerals like quartz or olivine. Especially in the range  
392 of low salinity, the concentration can be strongly underestimated if the pressure effect is  
393 ignored. Either pressure or salinity needs to be determined by an independent method. For  
394 experiments performed in diamond anvil cells with halogens in aqueous fluids, the change of  
395 Raman water band shifts can be a beneficial (with some restrictions) tool to monitor the  
396 pressure at room temperature, if salinity is known, and inversely this change can be used to  
397 monitor the salinity.

398

## 399 6. Acknowledgments

400 This project was funded by the ANR Projet de Recherche Collaborative VOLC-HAL-CLIM  
401 (Volcanic Halogens: from Deep Earth to Atmospheric Impacts), ANR-18-CE01-0018 (Hélène  
402 Bureau). Tobias Grützner is grateful for the EU Marie Skłodowska-Curie Fellowship “ExCliso”  
403 (Project ID 101017762). We thank K. Béneut for his support with the Raman laser we used  
404 for our experiments at the IMPMC and Y. Guarnelli for his help with the DAC alignment. We

405 are very grateful to E.A. Pankrushina for providing the raw dataset of Raman spectra from  
406 her study. We thank the two reviewers for their helpful comments to improve the manuscript  
407 and editor Claudia Romano is thanked for handling the manuscript.

408

409

410 Statement: During the preparation of this work the authors used ChatGPT 3.5 to correct  
411 errors of spelling, punctuation, grammar and to improve the syntax in several chapters of the  
412 manuscript. After using this tool, the authors reviewed and edited the content and take full  
413 responsibility for the content of the publication.

414

415 7. References

- 416 Aiuppa, A., Baker, D.R., & Webster, J.D., 2009. Halogens in volcanic systems. *Chem. Geol.*,  
417 **263(1-4)**, 1-18. <https://doi.org/10.1016/j.chemgeo.2008.10.005>.
- 418 Bakker, R.J., 2004. Raman spectra of fluid and crystal mixtures in the systems H<sub>2</sub>O, H<sub>2</sub>O-NaCl  
419 and H<sub>2</sub>O-MgCl<sub>2</sub> at low temperatures: applications to fluid-inclusion research. *Can. Mineral.*  
420 **42**, 1283-1314. <https://doi.org/10.2113/gscanmin.42.5.1283>.
- 421 Besemer, M., Bloemenkamp, R., Ariese, F., van Manen, H.-J., 2016. Identification of multiple  
422 water-iodide species in concentrated NaI solutions based on the raman bending vibration of  
423 water. *J. Phys. Chem. A* **120(5)**, 709-714. <https://doi.org/10.1021/acs.jpca.5b10102>.
- 424 Brooks, H.L., Dragovic, B., Lamadrid, H.M., Caddick, M.J., Bodnar, R.J., 2019. Fluid capture  
425 during exhumation of subducted lithologies: A fluid inclusion study from Sifnos, Greece.  
426 *Lithos* **332-333**, 120-134. <https://doi.org/10.1016/j.lithos.2019.01.014>.
- 427 Bureau, H., Keppler, H., and Métrich, N., 2000. Volcanic degassing of bromine and iodine:  
428 Experimental fluid/melt partitioning data and applications to stratospheric chemistry: *Earth*  
429 *Planet. Sci. Lett.* **183**, 51-60. [https://doi.org/10.1016/S0012-821X\(00\)00258-2](https://doi.org/10.1016/S0012-821X(00)00258-2).
- 430 Bureau, H., Foy, E., Raepsaet, C., Somogyi, A., Munsch, P., Simon, G., Kubsy, S., 2010.  
431 Bromine cycle in subduction zones through in situ Br monitoring in diamond anvil cells.  
432 *Geochim. Cosmochim. Acta* **74**, 3839–3850. <https://doi.org/10.1016/j.gca.2010.04.001>.
- 433 Bureau, H., Auzende, A.-L., Marocchi, M., Raepsaet, C., Munsch, P., Testemale, D., Mézouar,  
434 M., Kubsy, S., Carrière, M., Ricolleau, A., Fiquet, G., 2016. Modern and past volcanic  
435 degassing of Iodine. *Geochim. Cosmochim. Acta* **173**, 114–125.  
436 <https://doi.org/10.1016/j.gca.2015.10.017>.
- 437 Chervin, J.C, Canny B., Besson, J. M., Pruzan, P., 1995. A diamond anvil cell for IR  
438 microspectroscopy. *Rev. Sci. Instrum.* **66** (3), 2595-2598. <https://doi.org/10.1063/1.1145594>.

439 Chervin J.C., Canny B., Mancinelli M., 2001. Ruby-spheres as pressure gauge for optically  
440 transparent high pressure cells. *High Press. Res.* **21**, 305–314.  
441 <https://doi.org/10.1080/08957950108202589>.

442 Daniel, J.S., Solomon, S., Portmann, R.W., 1999. Stratospheric ozone destruction: The  
443 importance of bromine relative to chlorine. *J. Geophys. Res.* **104**, 23871-23880.  
444 <https://doi.org/10.1029/1999JD900381>.

445 Dubessy J., Lhomme, T., Boiron, M-C., Rull, F., 2002. Determination of Chlorinity in Aqueous  
446 Fluids Using Raman Spectroscopy of the Stretching Band of Water at Room Temperature:  
447 Application to Fluid Inclusions. *Appl. Spectrosc.* **56(1)**, 99-106.

448 Đuričković, I., Marchetti, M., Claverie, R., Bourson, P., Chassot, J-M., Fontana, M.D., 2010.  
449 Experimental study of NaCl aqueous solutions by Raman spectroscopy: Towards a new  
450 optical sensor. *Appl. Spectrosc.* **64(8)**, 853-857.  
451 <https://doi.org/10.1366/000370210792080984>.

452 Fehn, U., 2012. Tracing crustal fluids: Applications of natural <sup>129</sup>I and <sup>36</sup>Cl. *Annu. Rev. Earth  
453 Planet. Sci.* **40**, 45-67. <https://doi.org/10.1146/annurev-earth-042711-105528>.

454 Georgiev, G.M., Kalkanjiev, T.K., Petrov, V.P., Nickolov, Zh., 1984. Determination of Salts in  
455 Water Solutions by a Skewing Parameter of the Water Raman Band. *Appl. Spectrosc.* **38(4)**,  
456 593-595. <https://doi.org/10.1366/0003702844555106>.

457 Gerlach, T.M., 2004. Volcanic source of tropospheric ozone-depleting trace gases. *Geochem.  
458 Geophys. Geosyst.* **5**, Q09007. <https://doi.org/10.1029/2004GC000747>.

459 Grützner, T., Bureau, H., Boulard, E., Munsch, P., Guignot, N., Siebert, J., Guarnelli, Y., 2024.  
460 An in-situ experimental HP/HT study on bromine release from a natural basalt. *Chem. Geol.*  
461 **644**, 121869. <https://doi.org/10.1016/j.chemgeo.2023.121869>.

462 Johnson, L.H., Burgess, R., Turner, G., Milledge, H.J., Harris, J.W. 2000. Noble gas and  
463 halogen geochemistry of mantle fluids: comparison of African and Canadian diamonds.  
464 *Geochim. Cosmochim. Acta* **64**, 717-732. [https://doi.org/10.1016/S0016-7037\(99\)00336-1](https://doi.org/10.1016/S0016-7037(99)00336-1).

465 Journaux, B., Daniel, I., Caracas, R., Montagnac, G., Cardon, H., 2013. Influence of NaCl on  
466 ice VI and ice VII melting curves up to 6 GPa, implications for large icy moons. *Icarus* **226**,  
467 355-363. <https://doi.org/10.1016/j.icarus.2013.05.039>.

468 Kawamoto, T., Yoshikawa, M., Kumagai, Y., Mirabueno, M.H.T., Okuno, M., Kobayashi, T.,  
469 2013. Mantle wedge infiltrated with saline fluids from dehydration and decarbonation of  
470 subducting slab. *Proc. Nat. Acad. Sci. USA.*, **110(24)**, 9663-9668.  
471 <https://doi.org/10.1073/pnas.1302040110>.

472 Kawamoto, T., Mibe, K., Bureau, H., Reguer, S., Mocuta, C., Kubsy, S., Thiaudière, D., Ono,  
473 S., Kogiso, T., 2014. Large-ion lithophile elements delivered by saline fluids to the sub-arc  
474 mantle. *Earth Planets Space* **66**, 61. <https://doi.org/10.1186/1880-5981-66-61>.

475 Krishnamurthy, S., Bansil, R., Wiafe-Akente, J., 1983. Low-frequency Raman spectrum of  
476 supercooled water. *J. Chem. Phys.* **79**, 5863-5870. <https://doi.org/10.1063/1.445756>.

477 Leroy, C.; Bureau, H., Sanloup, C., Raepsaet, C., Glazirin, K., Munsch, P., Harmand, M.,  
478 Prouteau, G., Khodja, H., 2019. Xenon and iodine behaviour in magmas. *Earth. Planet. Sci.*  
479 *Lett.* **522**, 144-154. <https://doi.org/10.1016/j.epsl.2019.06.031>.

480 Louvel, M., Cadoux, A., Brooker, R.A., Proux, O., Hazemann, J-L., 2020a. New insights on Br  
481 speciation in volcanic glasses and structural controls on halogen degassing. *Am. Min.* **105**,  
482 795-802. <https://doi.org/10.2138/am-2020-7273>.

483 Louvel, M., Sanchez-Valle, C., Malfait, W.J., Pokrovski, G.S., Borca, C.N., Grolimund, D.,  
484 2020b. Bromine speciation and partitioning in slab-derived aqueous fluids and silicate melts  
485 and implications for halogen transfer in subduction zones. *Solid Earth* **11**, 1145-1161.  
486 <https://doi.org/10.5194/se-11-1145-2020>.

487 Mernagh, T.P., Wilde, A.R., 1989. The use of the laser Raman microprobe for the  
488 determination of salinity in fluid inclusions. *Geochim. Cosmochim. Acta* **53(4)**, 765-771.  
489 [https://doi.org/10.1016/0016-7037\(89\)90022-7](https://doi.org/10.1016/0016-7037(89)90022-7).

490 Moncada, D., Bodnar, R.J., 2012. Raman spectroscopy technique to determine the salinity of  
491 fluid inclusions, PACROFI-XI (Pan-American Current Research on Fluid Inclusions)  
492 Conference, pp. 67.

493 Ni, P., Ding, J., Rao, B., 2006. In situ cryogenic Raman spectroscopic studies on the synthetic  
494 fluid inclusions in the systems H<sub>2</sub>O and NaCl-H<sub>2</sub>O. *Chin. Sci. Bull.* **51(1)**, 108-114.  
495 <https://doi.org/10.1007/s11434-004-0256-5>.

496 Pankrushina, E.A., Krupenin, M.T., Shchapova, Y.V., Kobuzov, A.S., Garaeva, A.A., Votyakov,  
497 S.L., 2020. The study of fluid inclusion salinity in minerals by raman spectroscopy revisited.  
498 In: Votykov, S., Kiseleva, D., Grokhovsky, V., Shchapova, J. (eds.), *Minerals: Structure,*  
499 *Properties, Methods of Investigation: Proceedings of the 10th All-Russian Youth Scientific*  
500 *Conference* (pp. 175-183). Springer International Publishing. <https://doi.org/10.1007/978-3->  
501 [030-49468-1\\_23](https://doi.org/10.1007/978-3-030-49468-1_23).

502 Pyle, D.M., Mather, T.A., 2009. Halogens in igneous processes and their fluxes to the  
503 atmosphere and oceans from volcanic activity: A review. *Chem. Geol.* **263**, 110-121.  
504 <https://doi.org/10.1016/j.chemgeo.2008.11.013>.

505 Ratcliffe, C.I., Irish, D.E., 1982. Vibrational spectral studies at elevated temperatures and  
506 pressures. Raman studies of liquid water up to 300 °C. *J. Phys. Chem.* **86**, 4897-4905.  
507 <https://doi.org/10.1021/j100222a013>.

508 Romanenko, A.V., Rashchenko S.V., Goryainov, S.V., Likhacheva  
509 <https://doi.org/10.1177/0003702817752487>, A.Y., Korsakov, A.V., 2018. In Situ Raman  
510 Study of Liquid Water at High Pressure. *Appl. Spectrosc.* **72(6)**, 847-852.  
511 <https://doi.org/10.1177/0003702817752487>.

512 Shaw, T., Cooper, L., 1957. State of Iodine in Sea Water. *Nature* **180**, 250.  
513 <https://doi.org/10.1038/180250a0>.

514 Shen, G., Wang, Y., Dewaele, A., Wu, C., Fratanduono, D.E., Eggert, J., Klotz, S., Dziubek,  
515 K.F., Loubeyre, P., Fat'yanov, O.V., Asimov, P.D., Mashimo, T., Wentzcovitch, R.M.M., 2020.

516 Toward an international practical pressure scale: A proposal for an IPPS ruby gauge (IPPS-  
517 Ruby2020). *High Press. Res.* **40(3)**, 299-314.  
518 <https://doi.org/10.1080/08957959.2020.1791107>.

519 Sinnhuber, B.-M., Sheode, N., Sinnhuber, M., Chipperfield, M.P., Feng, W., 2009. The  
520 contribution of anthropogenic bromine emissions to past stratospheric ozone trends: A  
521 modelling study, *Atmos. Chem. Phys.*, **9(8)**, 2863-2871. [https://doi.org/10.5194/acp-9-2863-](https://doi.org/10.5194/acp-9-2863-2009)  
522 2009.

523 Sun, Q., 2009. The Raman OH stretching bands of liquid water. *Vib. Spectrosc.* **51**, 213-217.  
524 <https://doi.org/10.1016/j.vibspec.2009.05.002>.

525 Sun, Q., 2012. Raman spectroscopic study of the effects of dissolved NaCl on water structure.  
526 *Vib. Spectrosc.* **62**, 110-114. <https://doi.org/10.1016/j.vibspec.2012.05.007>.

527 Sun, Q., Zhao, L., Li, N., Liu, J., 2010. Raman spectroscopic study for the determination of Cl-  
528 concentration (molarity scale) in aqueous solutions: Application to fluid inclusions. *Chem.*  
529 *Geol.* **272(1-4)**, 55-61. <https://doi.org/10.1016/j.chemgeo.2010.02.004>.

530 Terpstra, P., Combes, D., Zwick, A., 1990. Effect of salts on dynamics of water: A Raman  
531 spectroscopy study. *J. Chem. Phys.* **92**, 65-70. <https://doi.org/10.1063/1.458418>.

532 Walrafen, G.E., Fisher, M.R., Hokmabadi, M.S., Yang, W.-H., 1986. Temperature dependence  
533 of the low- and high-frequency Raman scattering from liquid water. *J. Chem. Phys.* **85(12)**,  
534 6970-6982. <https://doi.org/10.1063/1.451384>.

535

536

537

## 8. Tables

	NaCl				max(NaCl) <sup>a</sup>
g/l	10	20	50	100	317
mol/l	0.17	0.34	0.86	1.71	5.42
wt.%	0.99	1.96	4.76	9.09	24.07

	NaBr				max(NaBr) <sup>a</sup>
g/l	20	50	100	150	905
mol/l	0.19	0.49	0.97	1.46	8.80
wt.%	1.96	4.76	9.09	13.04	47.51

	NaI			max(NaI) <sup>a</sup>
g/l	30	100	250	1793
mol/l	0.20	0.67	1.67	11.96
wt.%	2.91	9.09	20.00	64.20

<sup>a</sup> maximum solubility in H<sub>2</sub>O at 20 °C and ambient pressure.

538

539 *Table 1 Salt concentration in the starting solutions and maximum solubility values.*

540

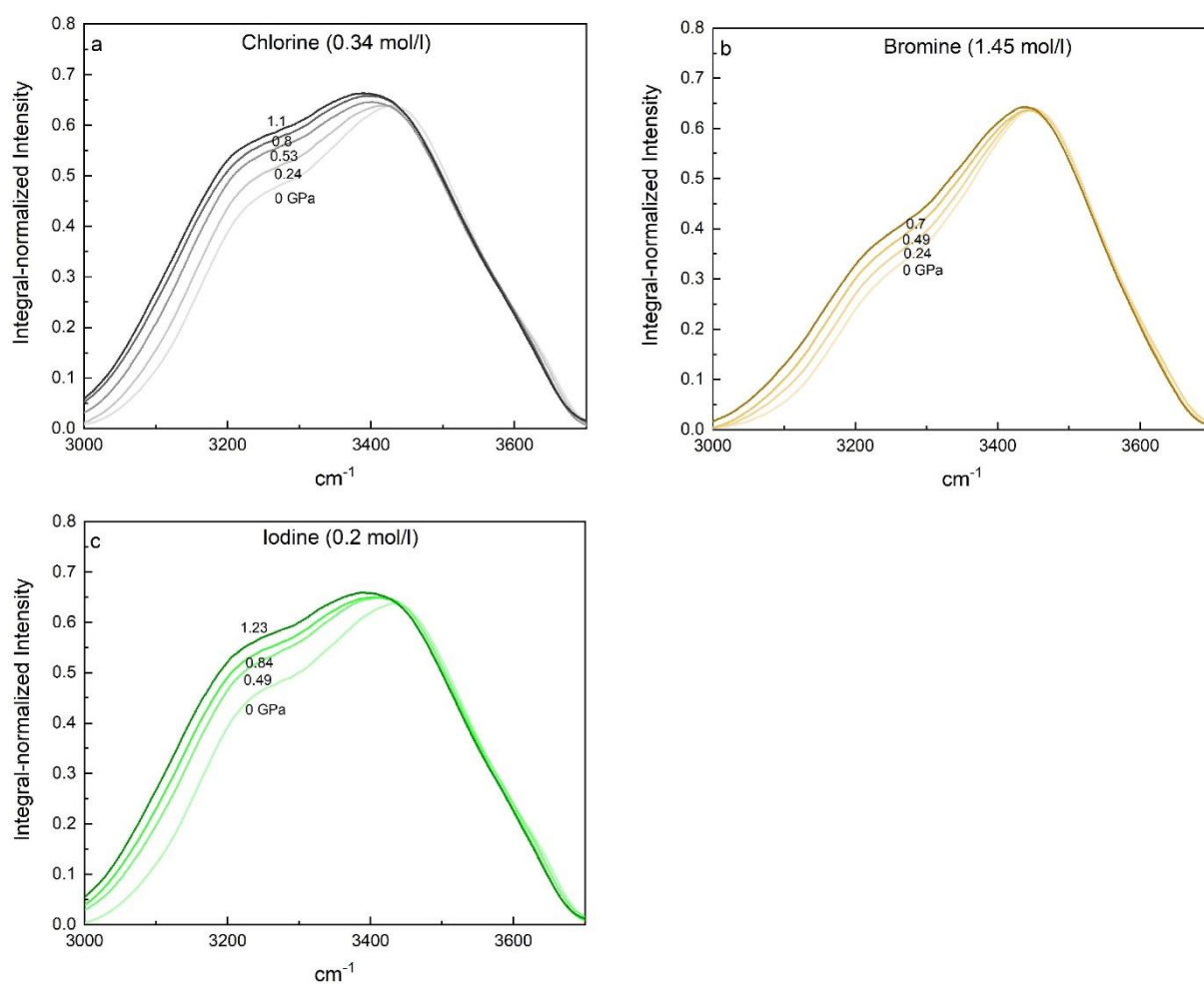
541



542 9. Supplementary material

543 Supplementary Tables with Raman raw data are stored under  
544 <https://data.mendeley.com/datasets/tnckfpjcv/1>.

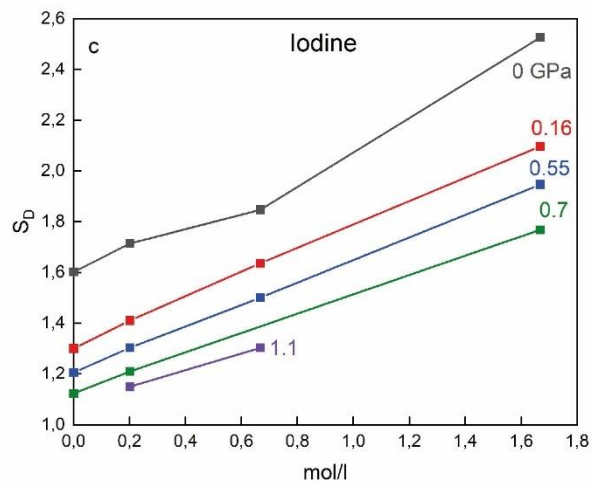
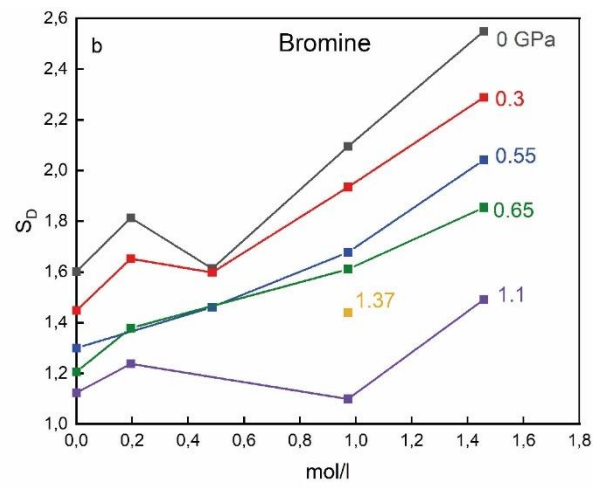
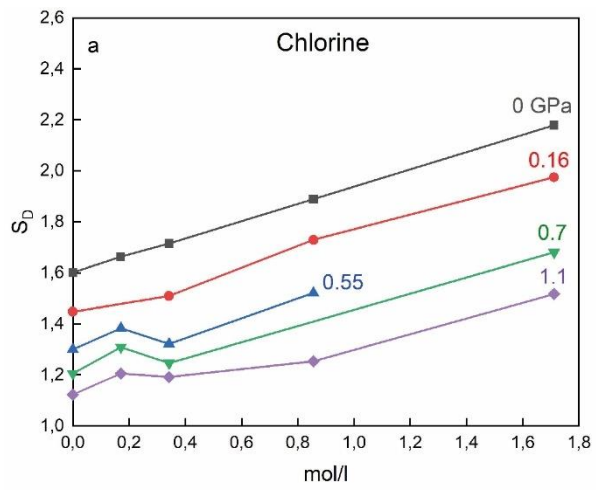
545



546

547 *Figure S1 The Raman water bands of saline solutions are presented with fixed halogen*  
548 *concentrations and varying pressure: a) 0.34 mol/l chlorine, b) 1.45 mol/l bromine, and c) 0.2*  
549 *mol/l iodine. The pressure is indicated in GPa on the spectra. Notably, the intensities are*  
550 *normalized to their integrated intensities for the presented range of 3000 to 3600  $\text{cm}^{-1}$ . The*  
551 *resulting peaks exhibit a smaller reduction than the spectra in Figure 3 but a leftward shift in*  
552 *the spectra indicates a clear pressure effect.*

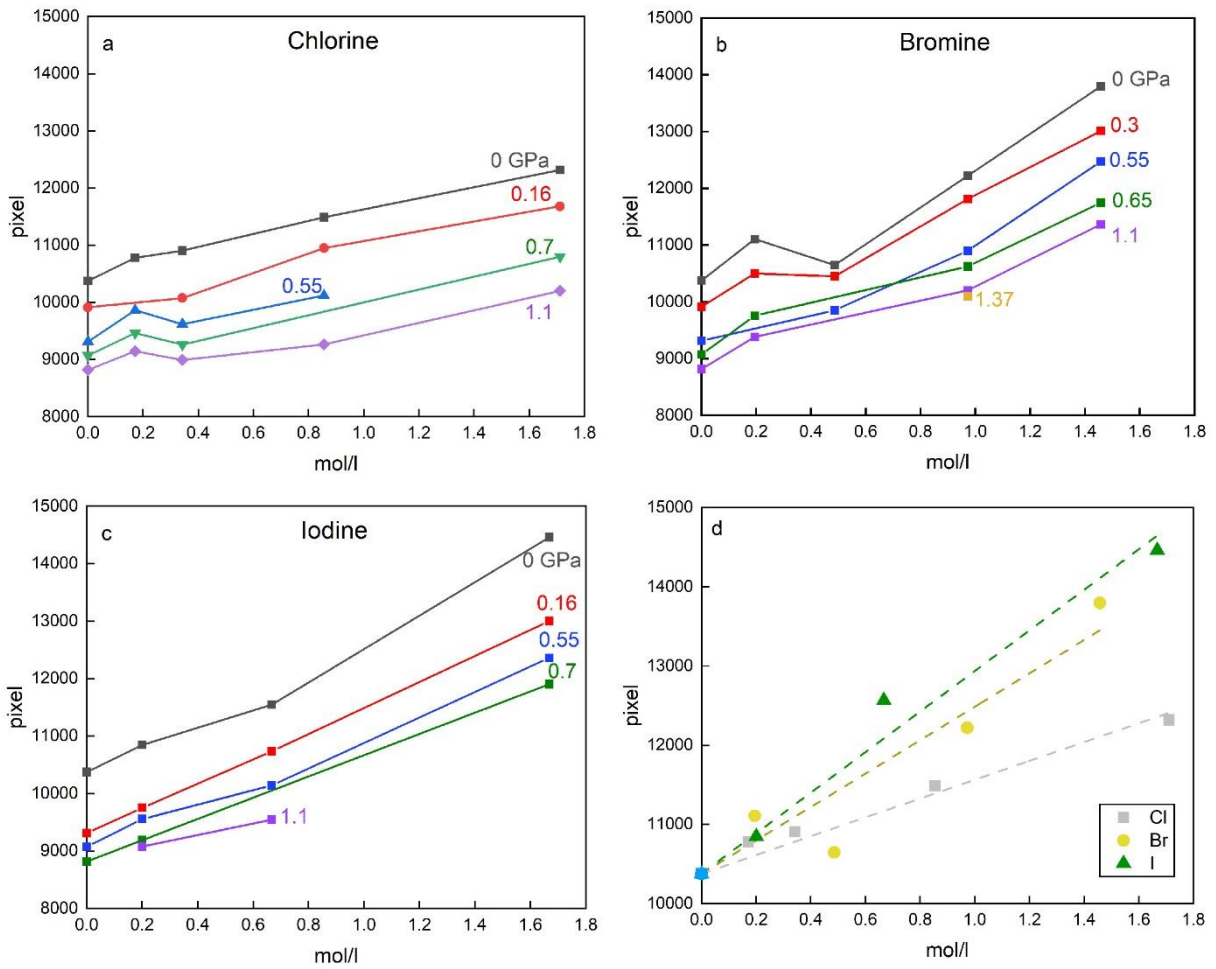
553



554

555 *Figure S2*  $S_D$  values vs halogen concentration for a) chlorine, b) bromine, and c) iodine  
 556 calculated after Durickovic et al. (2010).

557

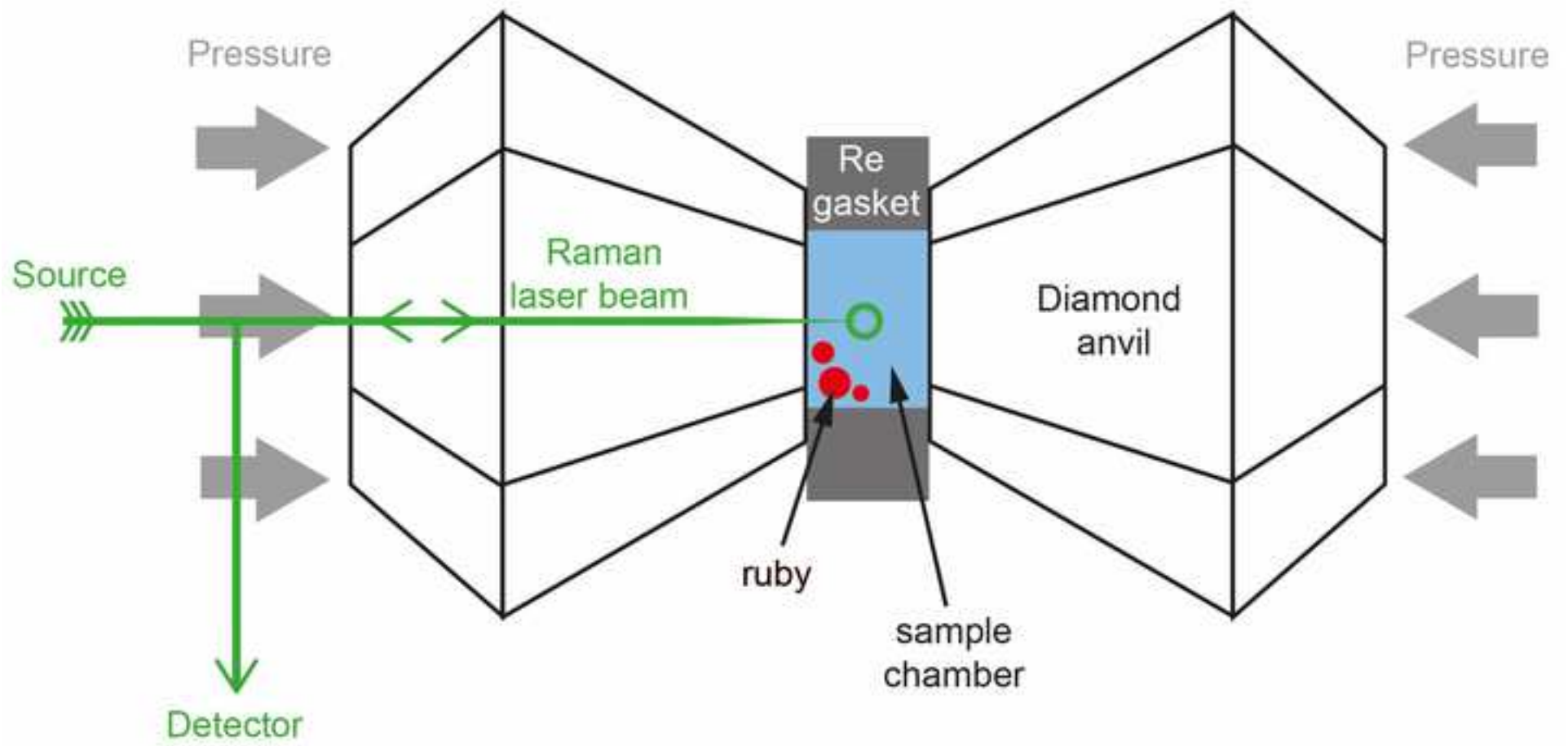


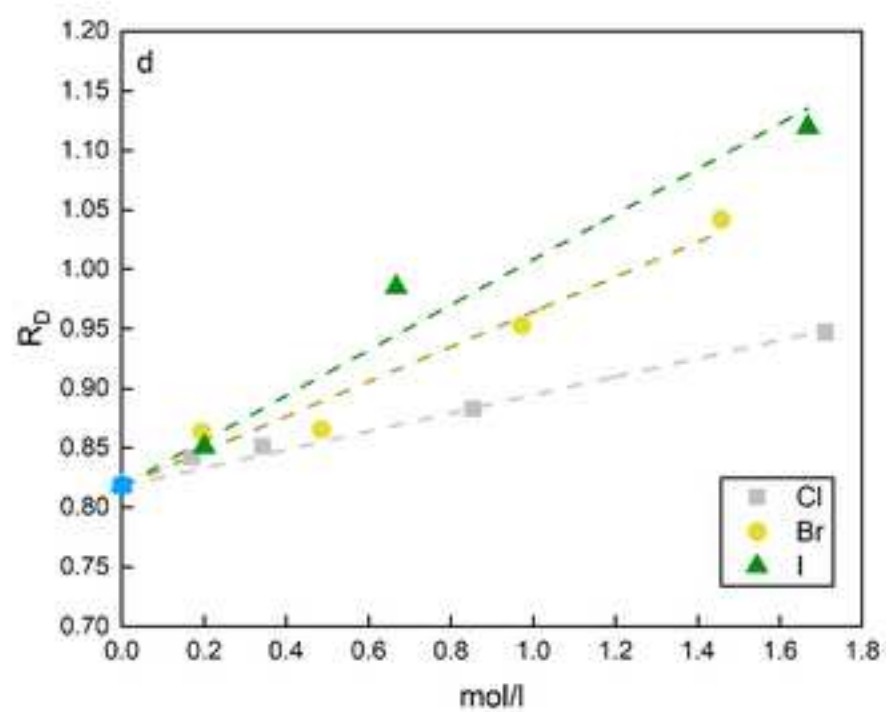
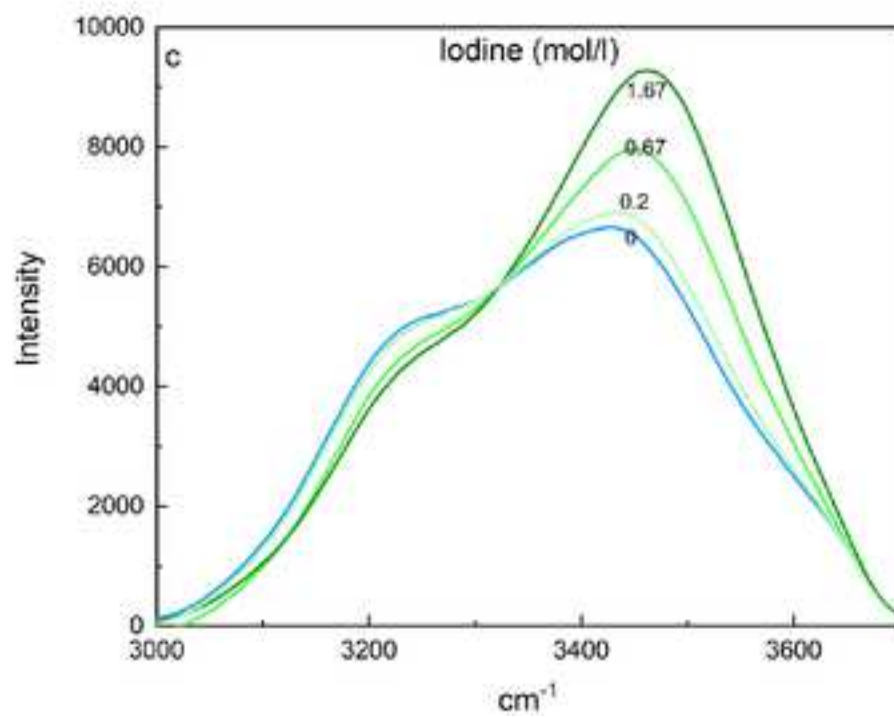
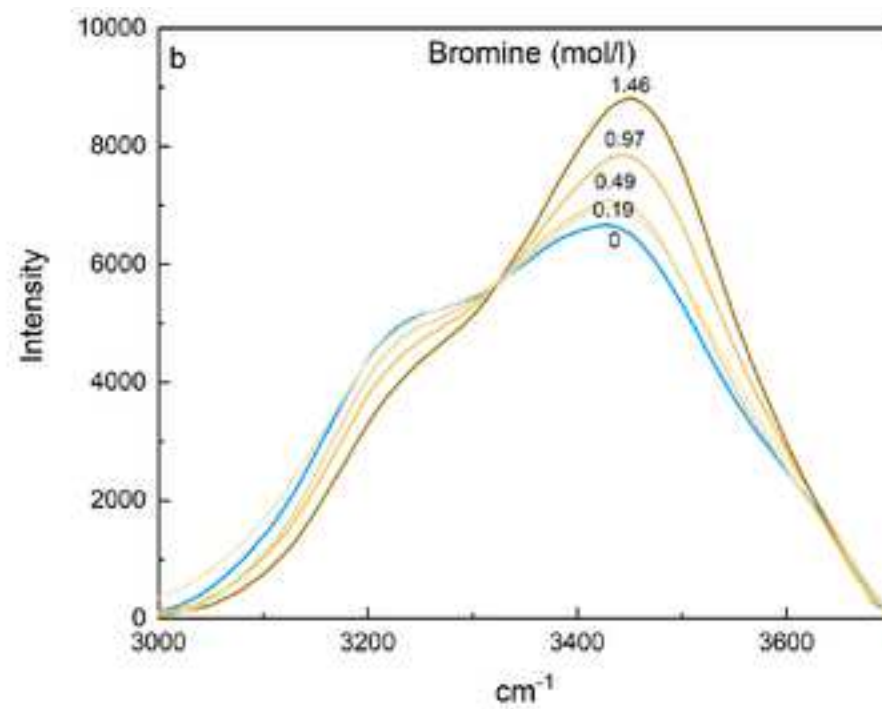
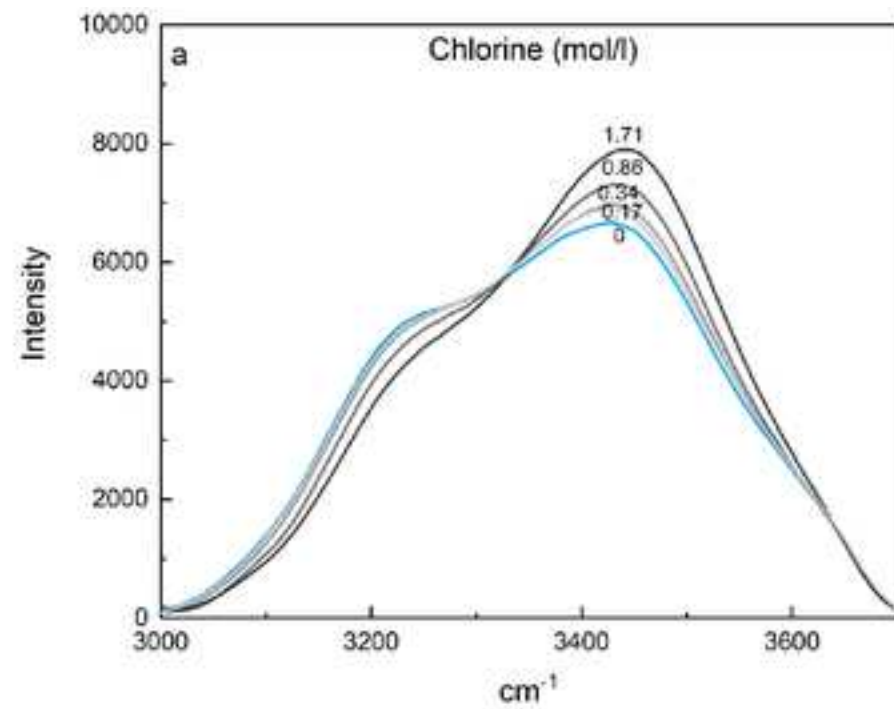
558

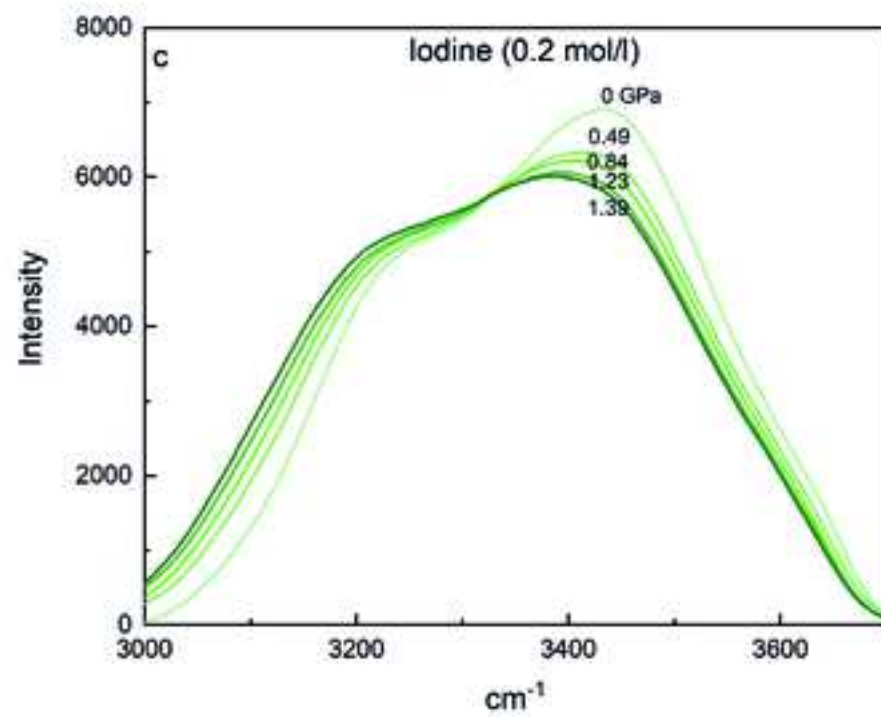
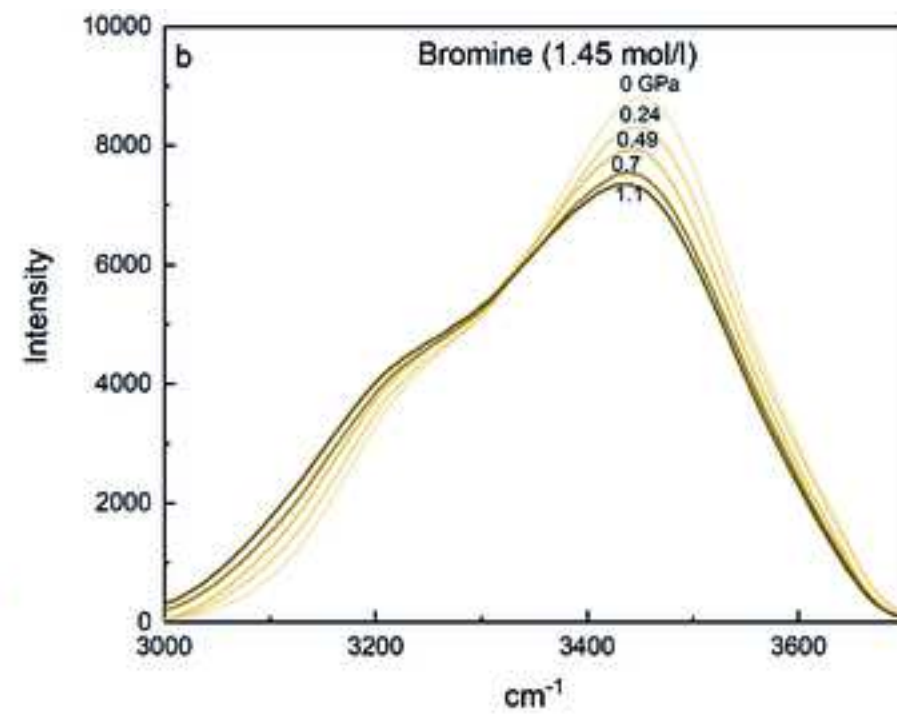
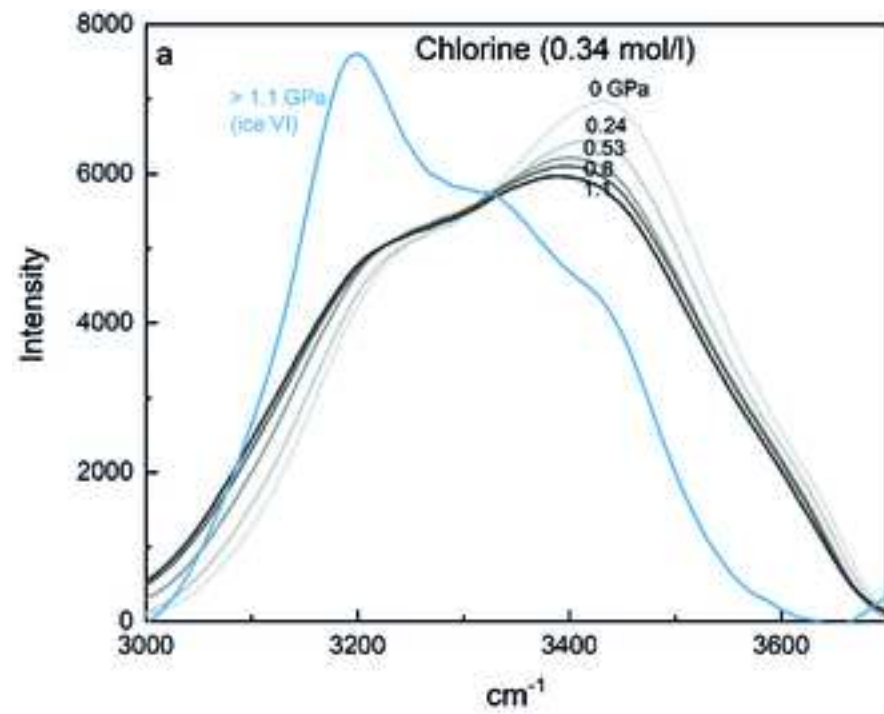
559 *Figure S3 Integrated intensities vs halogen concentration for (a) chlorine, (b) bromine, (c)*  
 560 *iodine, and (d) all three elements at ambient pressure show comparable trends but large*  
 561 *scatter relative to the  $R_D$  values. The intensities were integrated over the range of 3000 to 3600*  
 562  *$cm^{-1}$ .*

563

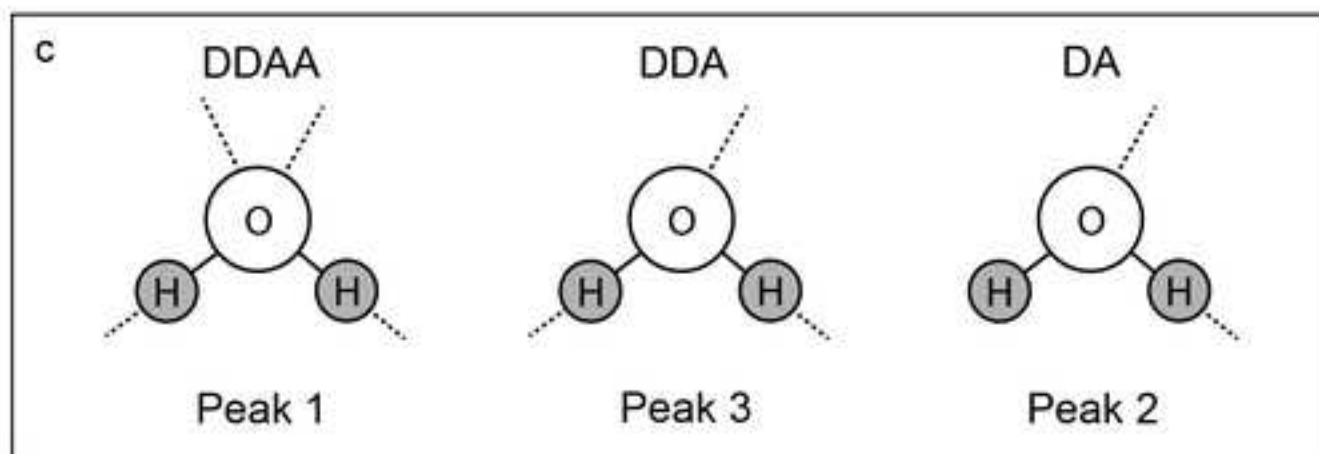
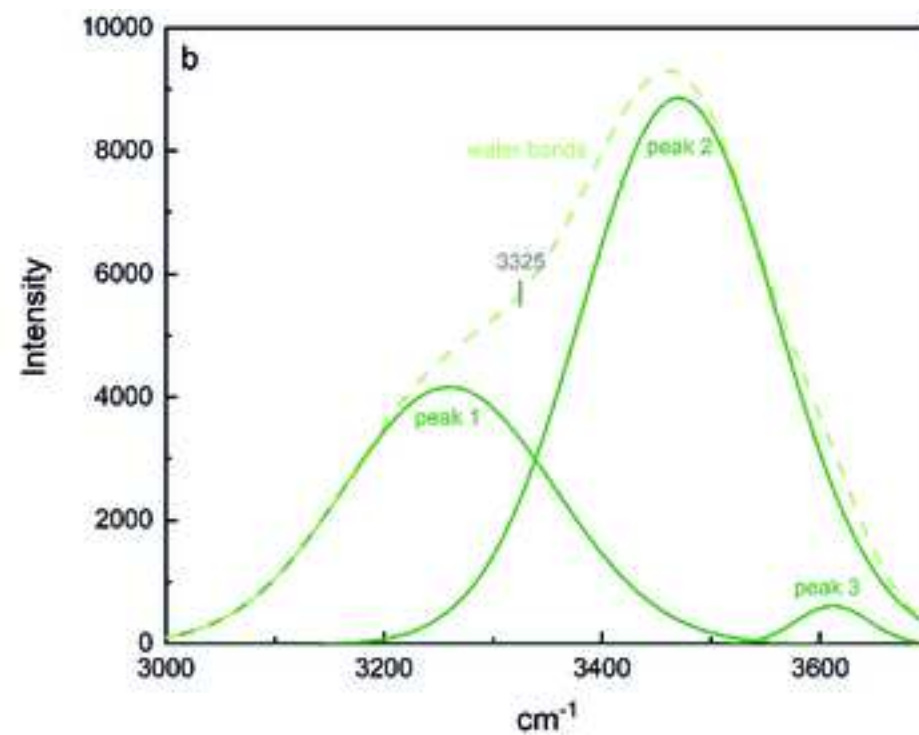
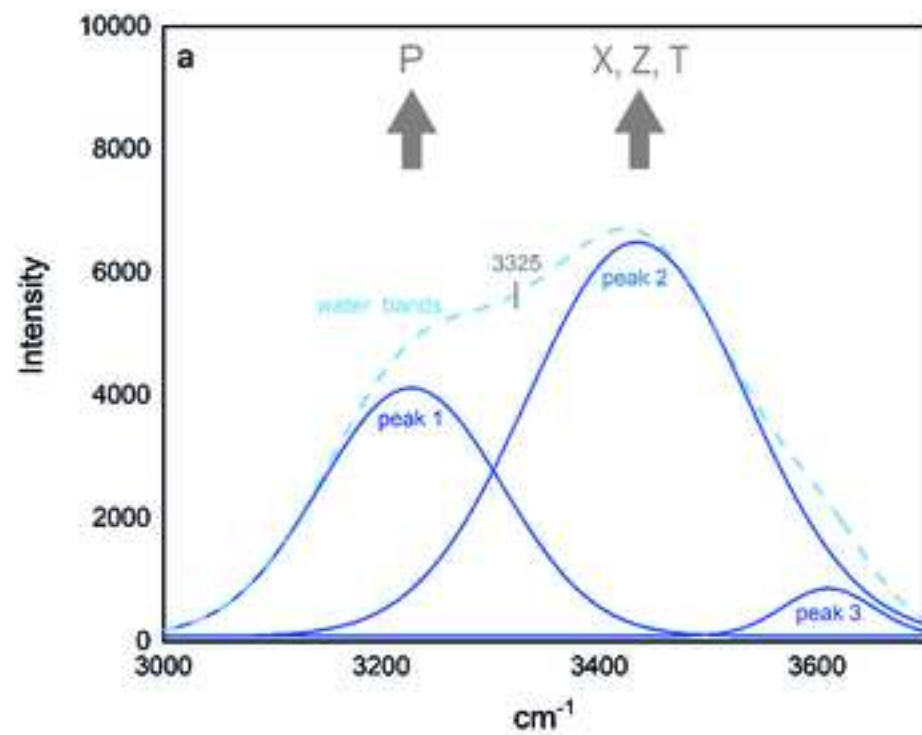
Figure 1

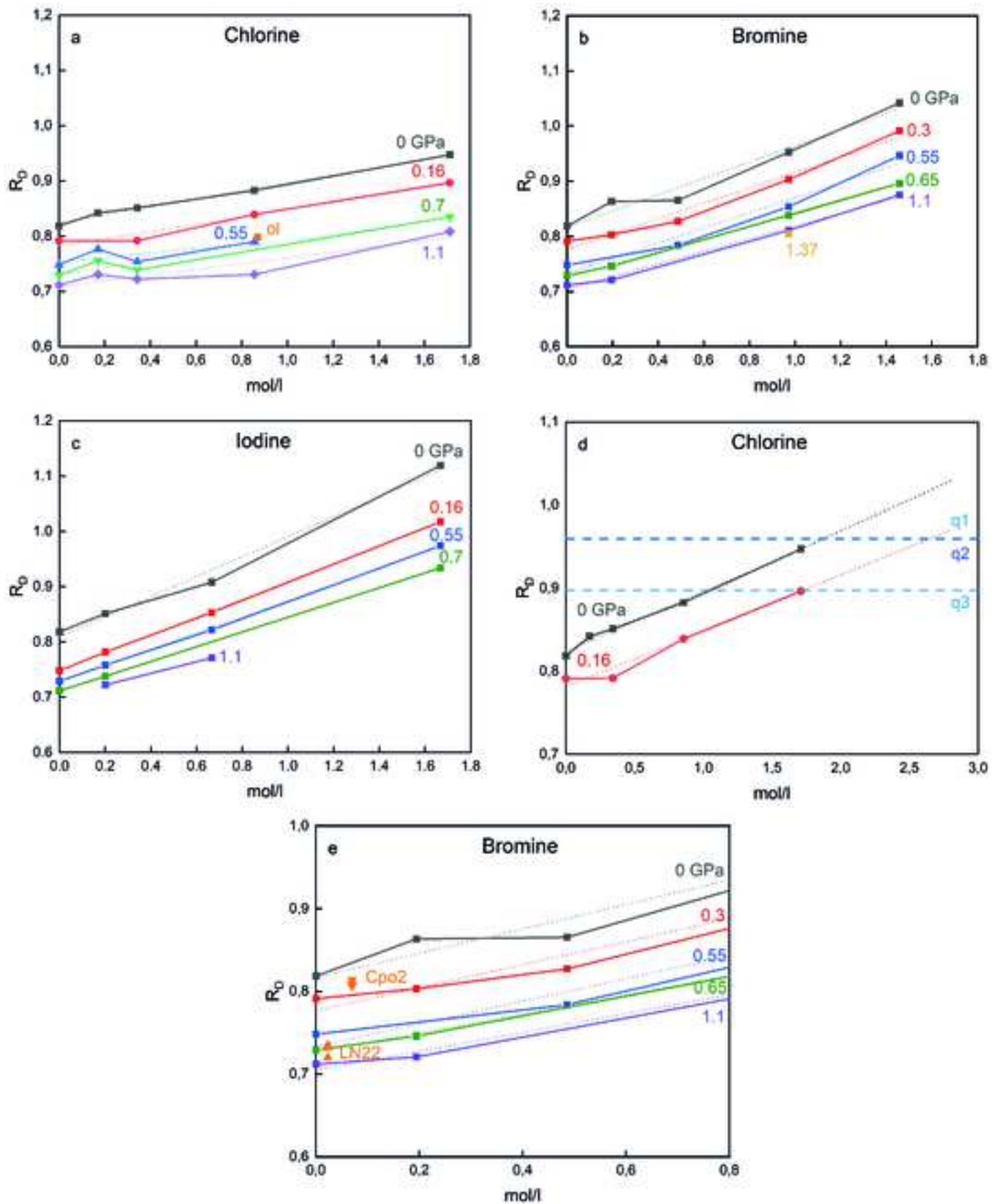




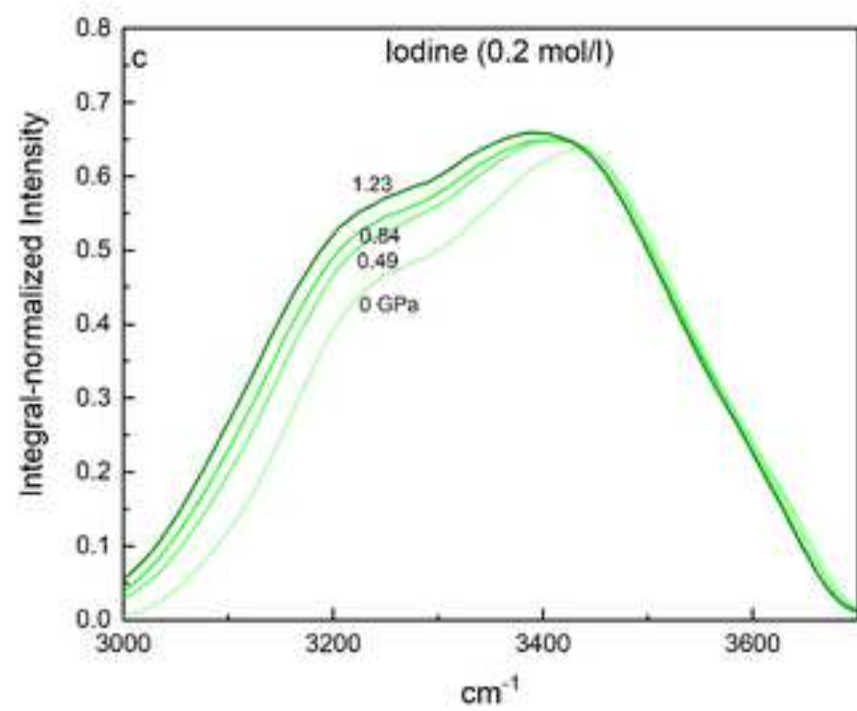
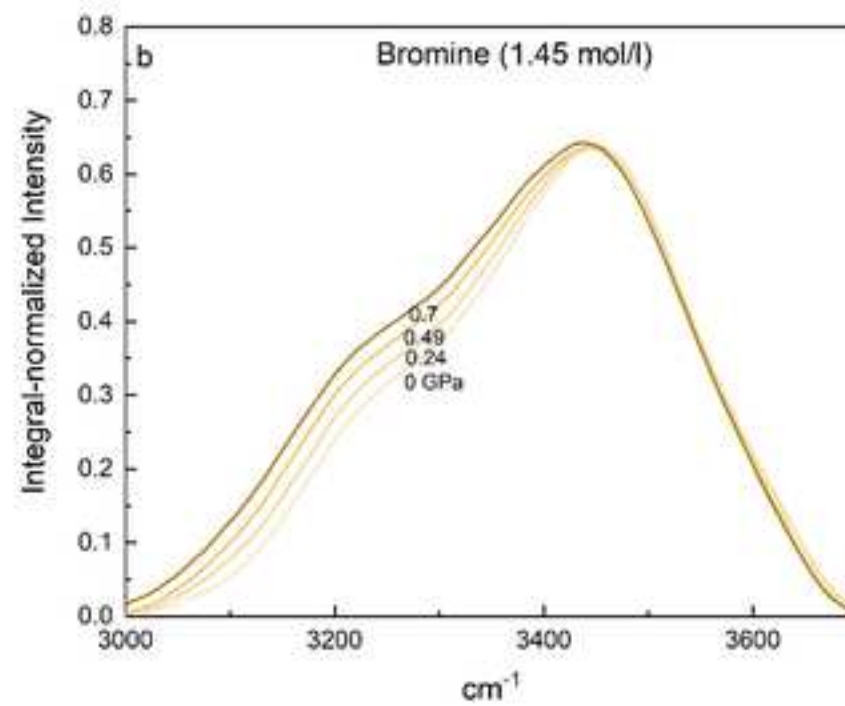
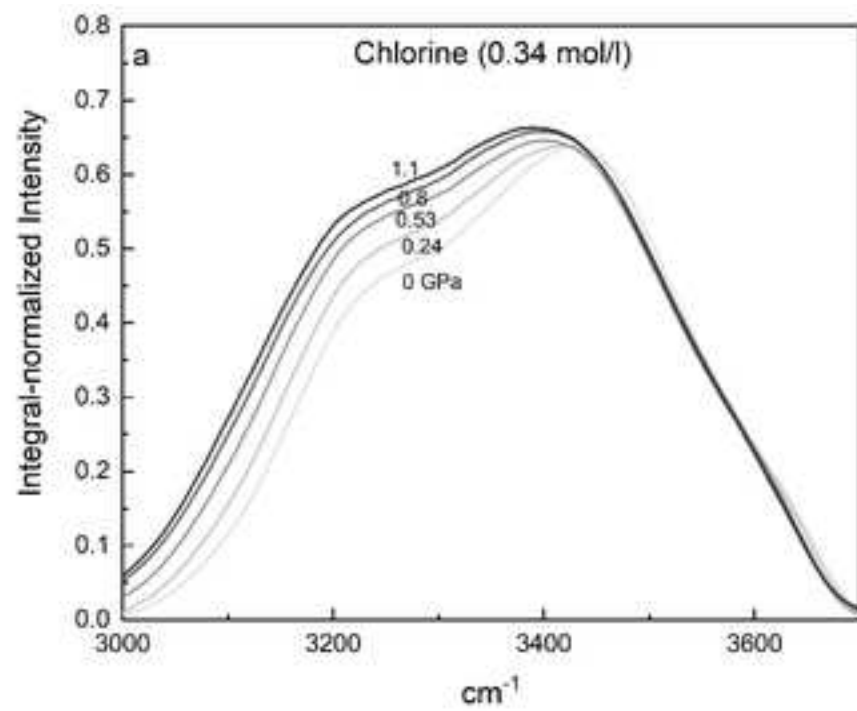


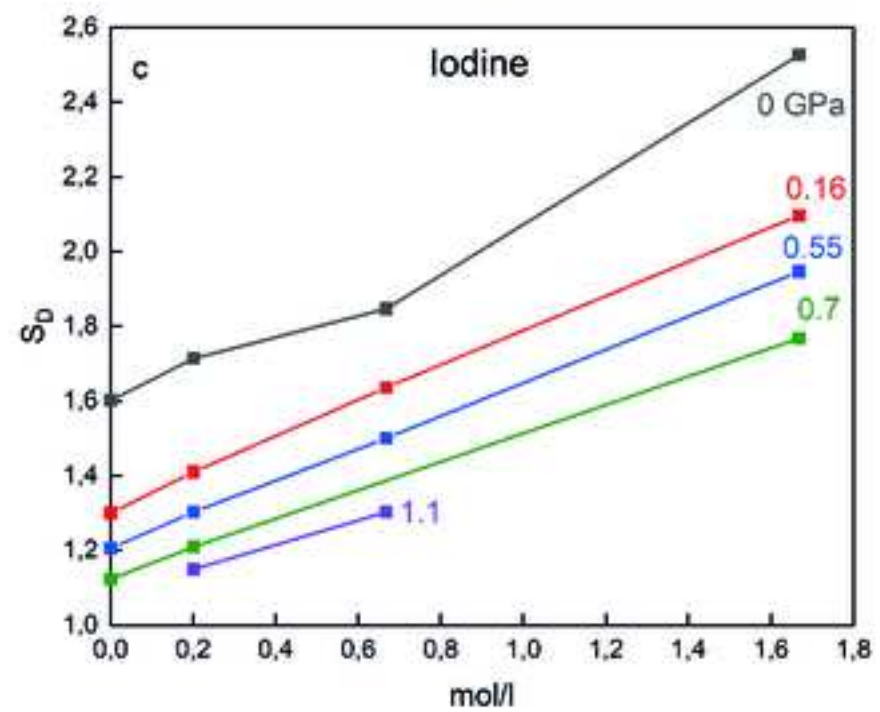
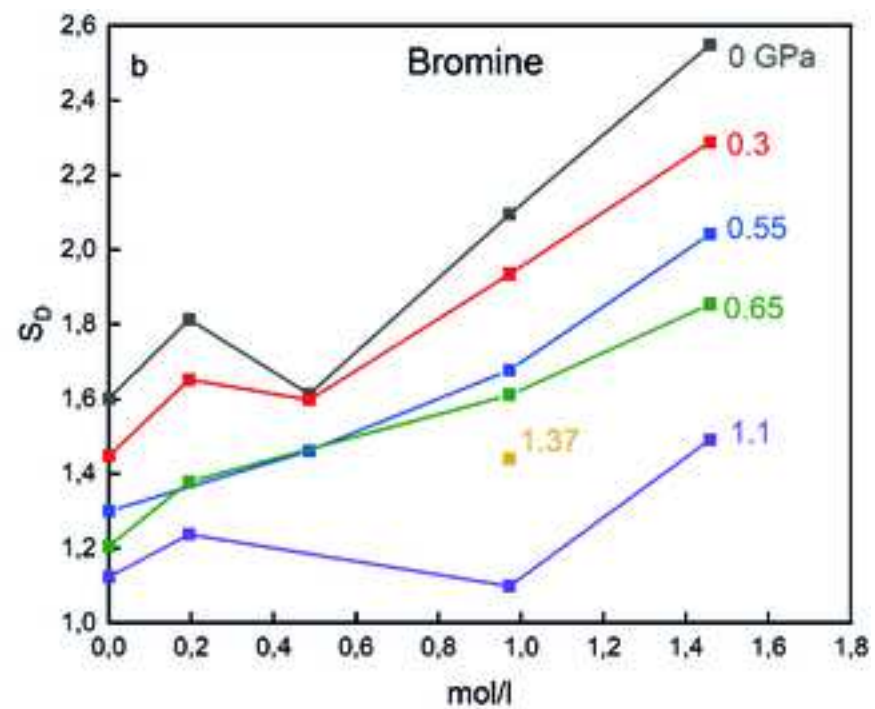
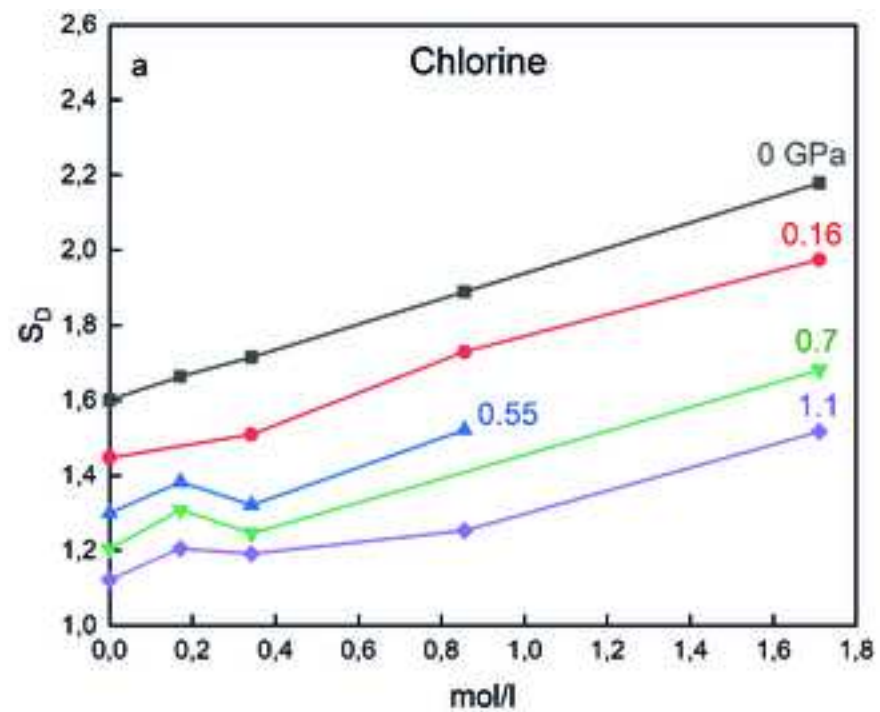












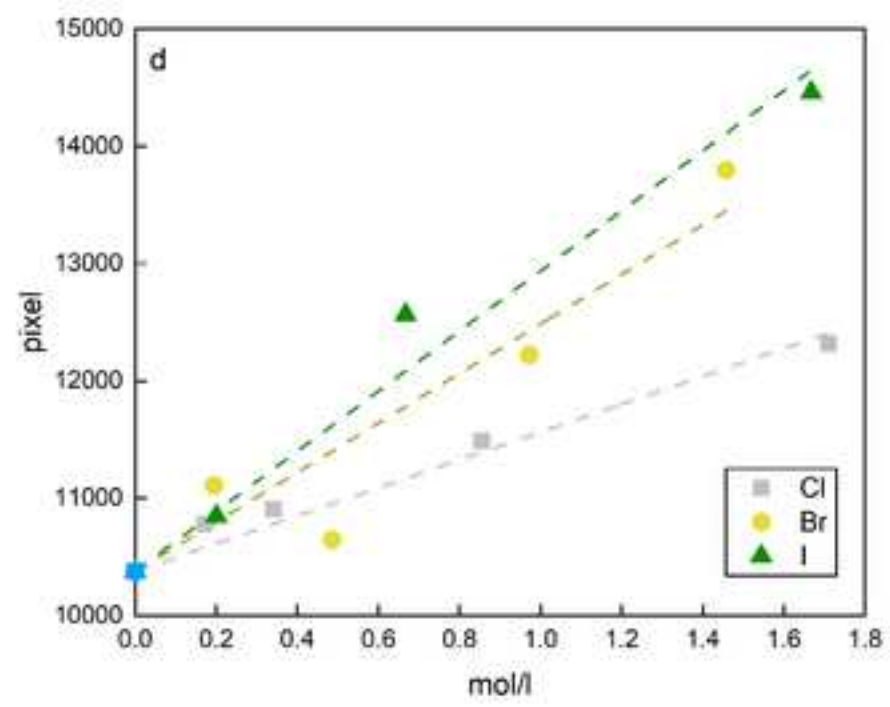
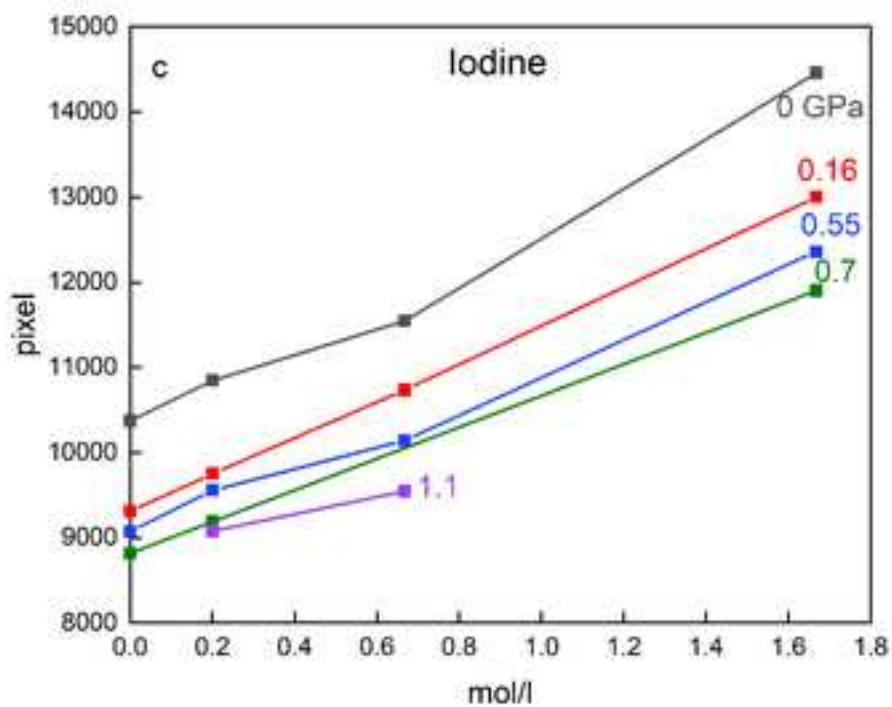
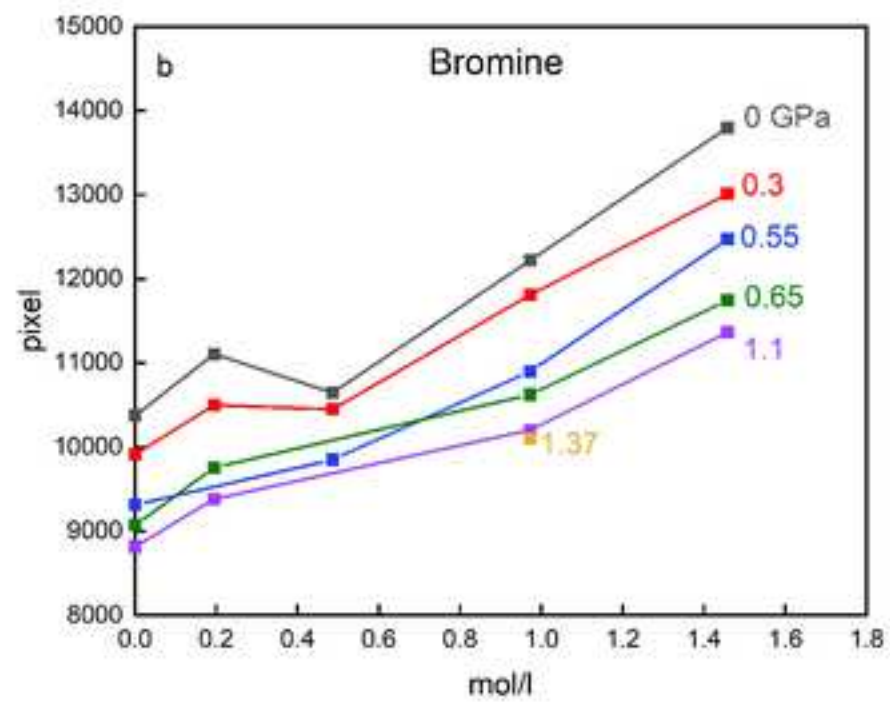
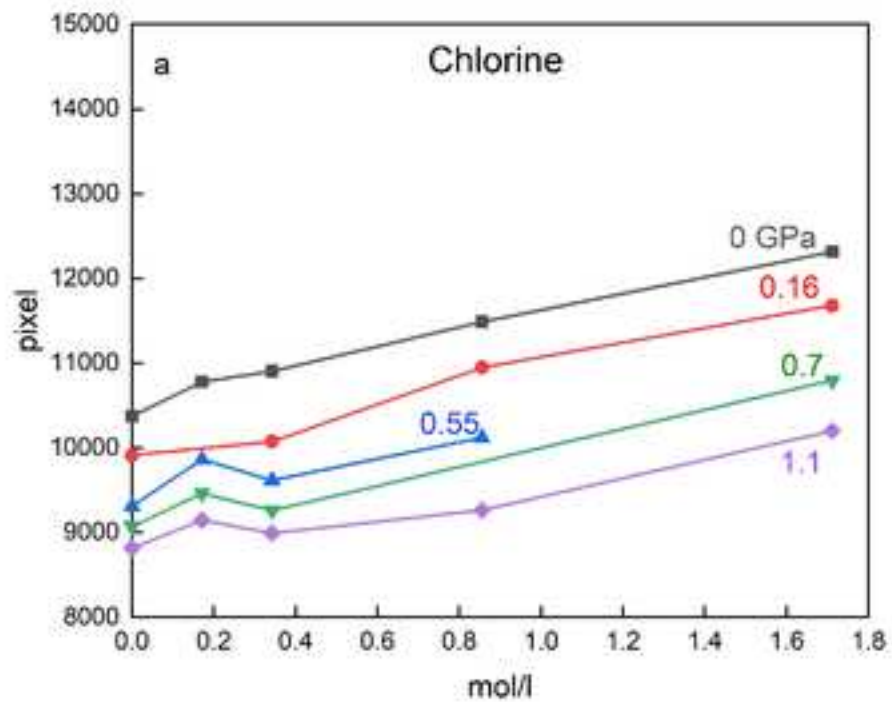


Table 1: Salt concentration in the starting solutions and maximum solubility values.

	NaCl				max(NaCl) <sup>a</sup>
g/l	10	20	50	100	317
mol/l	0.17	0.34	0.86	1.71	5.42
wt.%	0.99	1.96	4.76	9.09	24.07

	NaBr				max(NaBr) <sup>a</sup>
g/l	20	50	100	150	905
mol/l	0.19	0.49	0.97	1.46	8.80
wt.%	1.96	4.76	9.09	13.04	47.51

	NaI			max(NaI) <sup>a</sup>
g/l	30	100	250	1793
mol/l	0.20	0.67	1.67	11.96
wt.%	2.91	9.09	20.00	64.20

<sup>a</sup> maximum solubility in H<sub>2</sub>O at 20 °C and ambient pressure.

**Declaration of interests**

The authors declare that they have no known competing financial interests or personal relationships that could have appeared to influence the work reported in this paper.

The authors declare the following financial interests/personal relationships which may be considered as potential competing interests:

Tobias Grutzner reports financial support was provided by European Commission. Helene Bureau reports financial support was provided by French National Research Agency. If there are other authors, they declare that they have no known competing financial interests or personal relationships that could have appeared to influence the work reported in this paper.



Click here to download Research Data  
<https://data.mendeley.com/datasets/tnckfpjcv/1>

